nature microbiology

Article

https://doi.org/10.1038/s41564-023-01402-1

Plant commensal type VII secretion system causes iron leakage from roots to promote colonization

Received: 10 September 2022

Accepted: 4 May 2023

Published online: 29 May 2023

Check for updates

Yunpeng Liu[1,6] ✉, Xia Shu[1,2,3,6], Lin Chen[4,6], Huihui Zhang[2], Haichao Feng[2], Xiting Sun[1], Qin Xiong[1], Guangqi Li[1], Weibing Xun[2], Zhihui Xu[2], Nan Zhang[2], Corné M. J. Pieterse[5], Qirong Shen[2] & Ruifu Zhang[1,2] ✉

Competition for iron is an important factor for microbial niche establishment in the rhizosphere. Pathogenic and beneficial symbiotic bacteria use various secretion systems to interact with their hosts and acquire limited resources from the environment. *Bacillus* spp. are important plant commensals that encode a type VII secretion system (T7SS). However, the function of this secretion system in rhizobacteria–plant interactions is unclear. Here we use the beneficial rhizobacterium *Bacillus velezensis* SQR9 to show that the T7SS and the major secreted protein YukE are critical for root colonization. In planta experiments and liposome-based experiments demonstrate that secreted YukE inserts into the plant plasma membrane and causes root iron leakage in the early stage of inoculation. The increased availability of iron promotes root colonization by SQR9. Overall, our work reveals a previously undescribed role of the T7SS in a beneficial rhizobacterium to promote colonization and thus plant–microbe interactions.

Efficient colonization is necessary for microbes to exert potential virulent or beneficial functions on their host[1]. Due to the high diversity of and strong competition among soil microbes, rapid colonization is important for the occupation of nutrient-rich niches on roots by soil bacteria[2–4]. The plant growth-promoting rhizobacteria (PGPRs) have been widely used in agricultural production due to the multifunctional plant-beneficial properties[5,6]. These non-symbiotic beneficial rhizobacteria natively inhabit the rhizosphere and have been applied to benefit plants in a variety of ways, such as suppressing soil-borne disease, regulating plant development, enhancing stress tolerance, increasing nutrient availability[7] and stimulating plant immunity[8].

Iron plays a critical role in plant growth, development and defence and is also a limited resource in the rhizosphere, where the inhabiting microbes compete for this essential mineral nutrient[9,10]. Phytopathogens retrieve iron from their host cells, while plants utilize iron withholding strategies to fight against pathogen infections[10,11]. With their iron-mobilizing capacities, PGPRs can enhance plant iron uptake. Sufficient iron is also required for PGPRs to colonize and form biofilms on plant roots[12].

To establish an interaction with their hosts, a range of animal- and plant-associated pathogenic and symbiotic bacteria have developed distinct secretion systems that transfer certain proteins across the membrane or hydrophobic structures to the extracellular space[13,14].

[1]State Key Laboratory of Efficient Utilization of Arid and Semi-arid Arable Land in Northern China (the Institute of Agricultural Resources and Regional Planning, Chinese Academy of Agricultural Sciences, Beijing, China. [2]Jiangsu Provincial Key Lab for Organic Solid Waste Utilization, National Engineering Research Center for Organic-based Fertilizers, Jiangsu Collaborative Innovation Center for Solid Organic Waste Resource Utilization, Nanjing Agricultural University, Nanjing, P.R. China. [3]State Key Laboratory of Agricultural Microbiology, College of Life Science and Technology, Huazhong Agricultural University, Wuhan, China. [4]Experimental Center of Forestry in North China, Chinese Academy of Forestry, Beijing, P. R. China. [5]Plant-Microbe Interactions, Department of Biology, Utrecht University, Utrecht, the Netherlands. [6]These authors contributed equally to this study: Yunpeng Liu, Xia Shu, Lin Chen. ✉e-mail: liuyunpeng@caas.cn; rfzhang@njau.edu.cn

https://doi.org/10.1038/s41564-023-01402-1

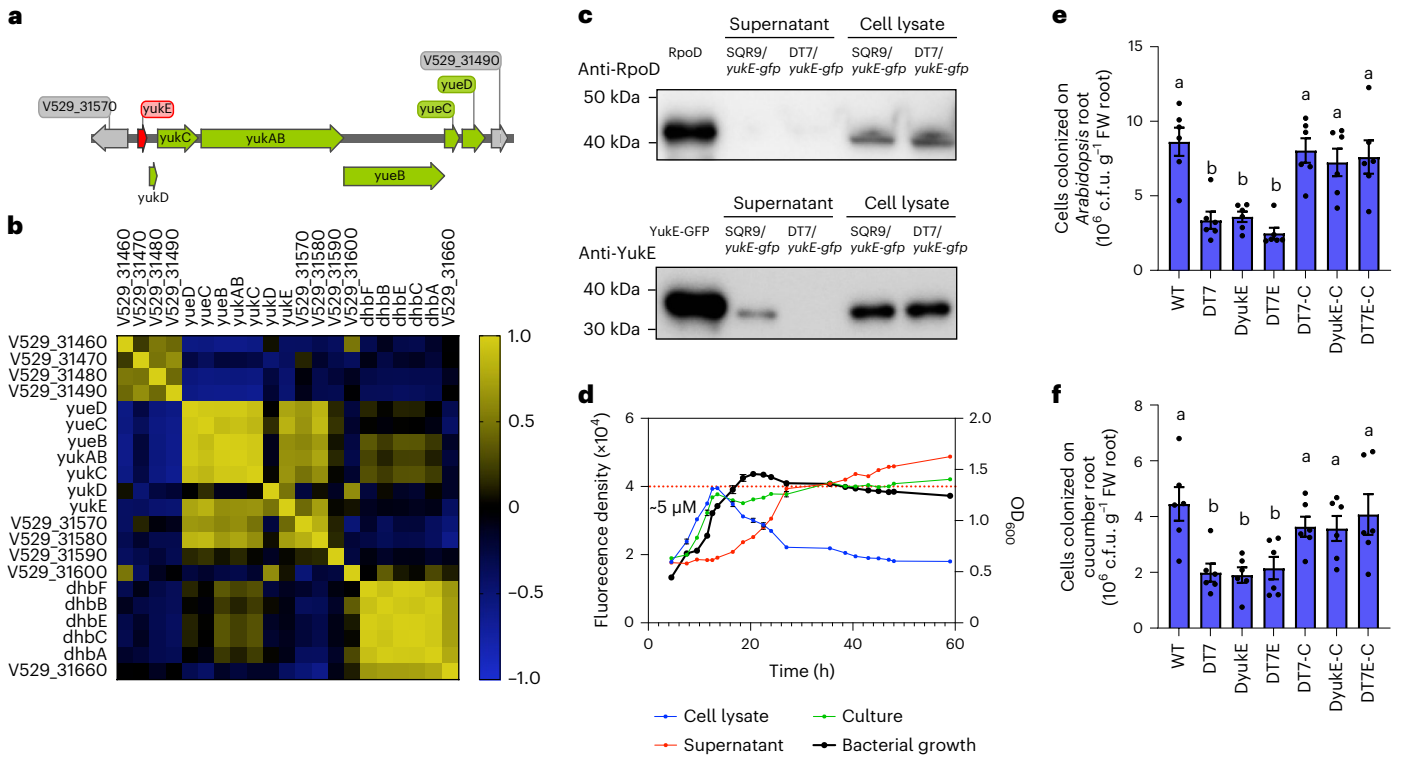

Fig. 1 | Contribution of the *B. velezensis* SQR9 tT7SS to root colonization. **a**, Schematic illustration of the *yuk/yue* operon encoding the T7SS. The red arrow indicates the gene encoding the secreted WXG100 family protein YukE, and the green arrow indicates the genes encoding the export machinery. **b**, Transcriptional correlation of the *yuk/yue* operon based on 72 RNA-seq data sets. Pearson correlation was calculated; colours indicate the *R* values of the transcriptional correlations between each pair of genes: yellow indicates high correlation, and blue indicates low correlation. **c**, Western blotting assay of the culture supernatants and cell lysates. The secretion property of YukE-GFP by SQR9 was verified by western blot with anti-YukE antibody and anti-RpoD antibody. RpoD, a constitutive cytoplastic protein, was detected by western blotting to indicate cell lysis. Purified YukE-GFP and RpoD were loaded at a final concentration of 20 μg ml^{-1}. Samples from the supernatant were prepared by TCA precipitation and dilution. Samples from cell lysates were prepared with collected cells treated with lysis buffer. The experiment was repeated two times with similar results. **d**, Content of YukE in the supernatant and cell lysate. The whole culture, supernatant and cell lysate from one sample were measured, and the OD_{600} was recorded to indicate cell density. Data are presented as mean ± s.e.m. ($n = 6$). The dotted line indicates the fluorescence density of 5 μM purified YukE-GFP. **e**,**f**, Colonization of WT SQR9, the mutants and the complementary strains on roots of *Arabidopsis* (**e**) and cucumber (**f**) grown in a hydroponic environment. Colonized bacterial cells were measured at 2 d post-inoculation. Fifteen-day-old *Arabidopsis* Col-0 plants and 21-day-old cucumber plants were used. Data are presented as mean ± s.e.m. Significant differences were determined with two-sided one-way ANOVA and Duncan's post-hoc test ($n = 6$, $\alpha = 0.05$, $P < 0.001$ for both **e** and **f**). The experiments with the mutants were repeated three times with similar results.

Among these systems, the type VII secretion system (T7SS) is unique to Firmicutes and Actinobacteria[15]. Recent studies revealed that EsxA, the core protein secreted by the T7SS of *Mycobacterium tuberculosis*, plays a central role in T7SS-mediated virulence, including the perturbation of phagosomal membranes[16–18]. T7SS is also conserved in *Bacillus* species[15], with the *yuk/yue* operon encoding the T7SS for secretion of YukE, which is homologous to EsxA in *Mycobacterium*[19–21]. So far, the biological and bioecological function of the *Bacillus* T7SS is unknown.

Bacillus velezensis SQR9 is a well-studied PGPR that colonizes roots and benefits plants by promoting growth and controlling disease[22–24]. *B. velezensis* SQR9 uses siderophores and specific iron ABC transporters to acquire iron, thereby supporting biofilm formation and root colonization[12]. In this study, we found that the T7SS of *B. velezensis* SQR9 and its secreted protein YukE cause iron leakage in plant roots, which contributes to root colonization by *B. velezensis* SQR9. We further revealed that the T7SS-secreted YukE might cause root iron leakage by direct insertion into the root plasma membrane.

Results

Bacterial T7SS contributes to root colonization

Genome analysis of *B. velezensis* SQR9 (China General Microbiology Culture Collection Center, CGMCC accession no. 5808) revealed that the *yuk* and *yue* clusters *yukE*, *yukD*, *yukC*, *yukAB*, *yueB*, *yueC*, *yueD* and *yueE* (V529_31490) constitute the T7SS coding region (Fig. 1a). On the basis of the collected RNA-seq results of 72 SQR9 samples from 5 independent projects (Supplementary Table 1)[25–28], we found a strong correlation between the transcriptional activities of *yueD*, *yueC*, *yueB*, *yukAB* and *yukC* (Fig. 1b). Transcription analysis indicated that *yukE*, *yukD*, *yukC*, *yukAB*, *yueB*, *yueC* and *yueD* are transcribed as polycistronic mRNAs (Supplementary Fig. 1), suggesting that they may all contribute to the function of the T7SS. YukE was reported to be the major protein secreted by the T7SS in *Bacillus*[19–21]. These transcriptional analyses demonstrate that YukE is one of the most highly transcribed genes (top 5 among 3,873 genes, Supplementary Table 1), suggesting an important role in *B. velezensis*.

To investigate the effect of the T7SS on root-rhizobacterium interactions, the T7SS-secreted protein gene *yukE*, genes of the type VII secretion machinery components (*yukD-yueD*) and the whole T7SS coding region (*yukD-yueD* and *yukE*) were deleted in *B. velezensis* SQR9. The resulting mutants, designated DyukE, DT7 and DT7E, respectively, were obtained, as well as their corresponding complementary strains, DyukE-C, DT7-C and DT7E-C. A GFP (green fluorescent protein) tag was fused in situ to the C terminus of YukE, and western blotting assays confirmed that wild-type (WT) SQR9 but not DT7 can secrete this

protein (Fig. 1c). By matching to a standard curve of purified YukE-GFP, the concentration of YukE-GFP secreted to the medium by SQR9 was calculated as 5 μM (Fig. 1d). Root colonization analysis of *Arabidopsis* and cucumber under hydroponic conditions showed that at 2 d post-inoculation, DyukE, DT7 and DT7E significantly reduced root colonization in *Arabidopsis*, while the complementary strains restored their colonization capacities (Fig. 1e,f). By using a well-controlled gnotobiotic FlowPot device (Extended Data Fig. 1a), *Arabidopsis* root colonization of these mutants and complementary strains was also compared with that of WT SQR9 in sterile soil (Extended Data Fig. 1b) and sterile soil inoculated with the soil-extracted microbial community (Extended Data Fig. 1c). The results from both conditions showed significant root colonization reduction of these mutants (Extended Data Fig. 1b,c), indicating that the function of T7SS on bacterial root colonization also works in the soil system, even in the presence of other microbes. Further evaluation with both *Arabidopsis* and cucumber in natural soil demonstrated that the T7SS and the secreted protein contributed to bacterial root colonization (Extended Data Fig. 1d,e). In addition, these mutants showed no significant differences from WT *B. velezensis* SQR9 in terms of growth, biofilm formation and motility, which are the factors affecting root colonization (Supplementary Figs. 2–4), suggesting that the T7SS and YukE contribute to root colonization by interacting with plants rather than by affecting bacterial properties.

B. velezensis decreases root iron content via T7SS

To explore the mechanism by which the T7SS and YukE affect root colonization by *B. velezensis* SQR9, RNA-seq was performed on *Arabidopsis* roots. YukE was exogenously expressed and purified, and heat-treated YukE (boiling water bath) was included as the negative control, which showed precipitation and changed structure as characterized by Fourier transform infrared spectroscopy (FTIR) and native polyacrylamide gel electrophoresis (PAGE) (Supplementary Fig. 5a–f and Table 3). YukE or heat-treated YukE was applied to the rhizosphere at a final concentration of 5 μM, and the root was sampled for RNA-seq at 1 h, 3 h, 6 h and 24 h post-treatment. We found that differentially expressed genes (DEGs) identified in the YukE treatment but not in the heat-treated YukE significantly ($q < 0.05$) enriched keywords for iron, haem, oxidoreductase and monooxygenase, and Gene Ontology (GO) molecular function categories iron ion binding, oxidoreductase activity, transcription factor activity and oxygen binding based on analysis using DAVID (DAVID Bioinformatics Resources 6.8) (Extended Data Fig. 2a and Supplementary Table 2). As most of the enriched keywords and GO categories are related to iron, we then performed RT–qPCR (Real time-quantitative PCR) to verify whether key genes of the plant iron deficiency response, such as *FIT, FRO2* and *IRT1* (Extended Data Fig. 2b), were affected in roots colonized by *B. velezensis* SQR9. *FIT* encodes a regulator of the iron deficiency response[29]. At 6 h and 24 h, the expression of *FIT* in the DT7-, DyukE- and DT7E-treated roots was significantly higher than in the WT *B. velezensis* SQR9-treated roots (Extended Data Fig. 2c). Consistently, the downstream genes *IRT1* and *FRO2* showed the same expression profiles (Extended Data Fig. 2d,e).

Iron is also a critical factor influencing plant immunity[10]. Iron has been shown to be involved in plant immunity through various mechanisms: (1) plant hosts can withhold iron from bacteria by restricting the iron sources in the apoplast, for example, by upregulating the iron storage protein FER1[30,31]; (2) iron deficiency can induce the RPS4-BTS-EDS1 pathway and mediate effector triggered immunity[32] to produce a cytoplasmic iron-dependent oxidative burst[11,33,34]; and (3) rhizobacteria-mediated induced systemic resistance has been shown to be associated with the upregulation of the iron deficiency response in plant roots. Induced systemic resistance is regulated by the root-specific transcription factor MYB72 which, as part of the iron deficiency response, regulates the biosynthesis and secretion of iron-mobilizing coumarins into the rhizosphere[35–38]. Our RT–qPCR results for *Arabidopsis* roots showed that *BTS*, *EDS1* and *RPS4* were not upregulated upon inoculation with either WT *B. velezensis* SQR9 or its derived mutants (Supplementary Fig. 6). Plant roots inoculated with WT *B. velezensis* SQR9 or any of its derived mutants induced the accumulation of O_2^- as shown by NBT staining, but no difference was observed between these treatments (Supplementary Fig. 7). Interestingly, *FER1*, the transcription factor gene *MYB72* and its downstream target *BGLU42* were differentially expressed in response to WT *B. velezensis* SQR9 and its derived mutants (Supplementary Fig. 8). At 24 h post-inoculation, the expression of *MYB72* and *BGLU42* in *B. velezensis* SQR9-inoculated roots was significantly lower than that in roots inoculated with DT7, DyukE and DT7E. The expression of *MYB72* was positively controlled by FIT[29]. As expected, *FIT* showed a similar expression profile as *MYB72* and *BGLU42* at 24 h post-inoculation (Extended Data Fig. 2c and Supplementary Fig. 8). These results confirmed that the T7SS of SQR9 plays a role in changing the local iron homoeostasis in colonized *Arabidopsis* roots.

The plant iron content was measured by Perls staining assays and inductively coupled plasma-mass spectrometry (ICP-MS). The Perls staining results showed that WT *B. velezensis* SQR9 dramatically decreased iron staining at 24 h post-inoculation (Fig. 2a–c and Supplementary Fig. 9). Compared with WT SQR9, mutants DT7, DyukE and DT7E all compromised this decreasing effect on iron staining. Interestingly, purified YukE but not heat-treated YukE decreased root iron staining at 24 h post-treatment, as did WT SQR9 (Fig. 2a–c). Moreover, purified YukE, but not heat-treated YukE, rescued the compromised function of root iron-decreasing of DT7, DyukE and DT7E in the Perls staining assay (Fig. 3a–c). These results indicate that *B. velezensis* SQR9 may cause a reduction in root iron content in a T7SS- and YukE-dependent manner. The *Arabidopsis* root iron content measured by ICP–MS at 12 h and 24 h post-inoculation or treatment showed that

Fig. 2 | Effect of the SQR9-derived strain and YukE on plant iron content. **a**, Image of Perls staining of 15-day-old *Arabidopsis* roots inoculated with *B. velezensis* SQR9 or treated with YukE. $n = 3$ independent replicates. This experiment was repeated twice with similar results. Blue staining represents iron. **b**, Microscopic view of Perls staining of iron in the roots of 15-day-old *Arabidopsis* at 24 h post-inoculation. For each treatment, the maturation zone of 12 roots was examined. The fraction under each image indicates the number of times the roots were successfully stained by Perls (with more than 300000 blue pixels in a 1.5 mm root) relative to the number of examined images. Scale bar, 100 μm. This experiment was repeated three times with similar results. **c**, Quantitative analysis of the Perls staining in **b**. Data are presented as mean ± s.e.m. Different letters above the bar indicate significant differences determined with two-sided one-way ANOVA and Duncan's post-hoc test ($n = 12$, $\alpha = 0.05$, $P < 0.001$). CK indicates the untreated plant. **d**–**f**, ICP–MS measurement of the iron content in roots of 15-day-old *Arabidopsis* treated with YukE- or SQR9-derived strains at 12 h (**d**), 24 h (**e**) and 48 h (**f**). $P = 0.815$ post-inoculation. Data are presented as mean ± s.e.m. Different letters above the bar indicate significant differences determined with two-sided one-way ANOVA and Duncan's post-hoc test ($n = 3$, $\alpha = 0.05$, $P < 0.001$ for **d**–**f**). This experiment was repeated twice with similar results. **g**, Effect of a gradient dose of YukE on 15-day-old *Arabidopsis* root iron content at 12 h post-inoculation measured by ICP–MS. Data are presented as mean ± s.e.m. Different letters above the bar indicate significant differences determined with two-sided one-way ANOVA and Duncan's post-hoc test ($n = 3$, $\alpha = 0.05$, $P < 0.001$). **h**, Effect of K252a and BFA on the root cell iron-decreasing capability of YukE at 24 h post-inoculation. For each treatment, 12 roots were examined. Scale bar, 100 μm. The fraction under each image indicates the number of times the roots were successfully stained by Perls (with more than 300000 blue pixels in a 1.5 mm root) relative to the number of examined images. This experiment was repeated twice with similar results. **i**. Quantitative analysis of the Perls staining of the root maturation zone in **h**. Data are presented as mean ± s.e.m. ($n = 3$). Different letters above the bar indicate significant differences determined with two-sided one-way ANOVA and Duncan's post-hoc test ($n = 12$, $\alpha = 0.05$, $P < 0.001$).

https://doi.org/10.1038/s41564-023-01402-1

WT SQR9 and purified YukE decreased the root iron content, while DT7, DyukE and DT7E did not (Fig. 2d,e), which is similar to the Perls staining results. In addition, the complementary strains decreased the root iron content, similar to WT SQR9 (Fig. 2d,e). A purified mutated protein, YukE^{S38C} (Supplementary Fig. 5g), also failed to decrease the root iron content (Fig. 2d,e), indicating that the effect of YukE on the

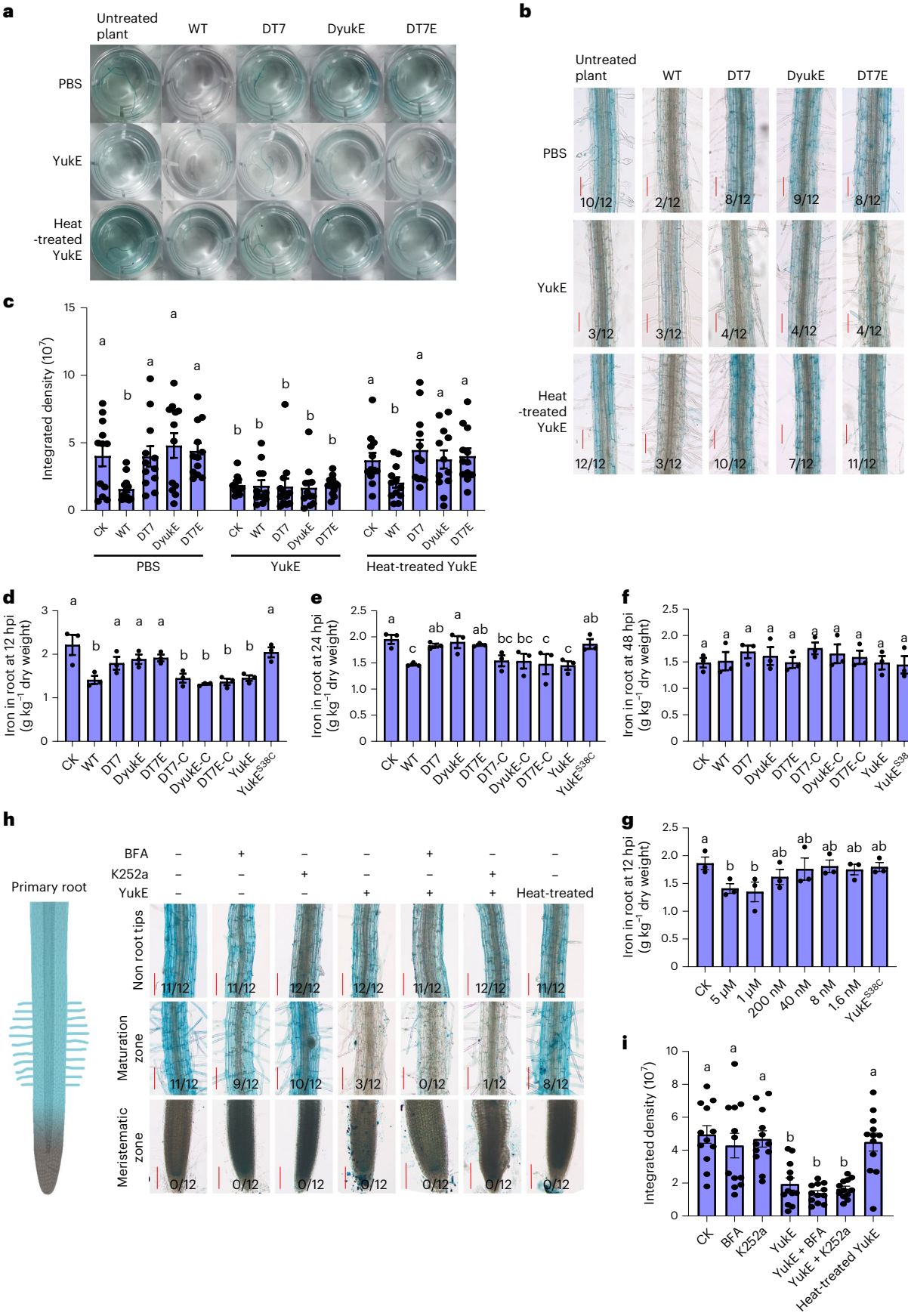

https://doi.org/10.1038/s41564-023-01402-1

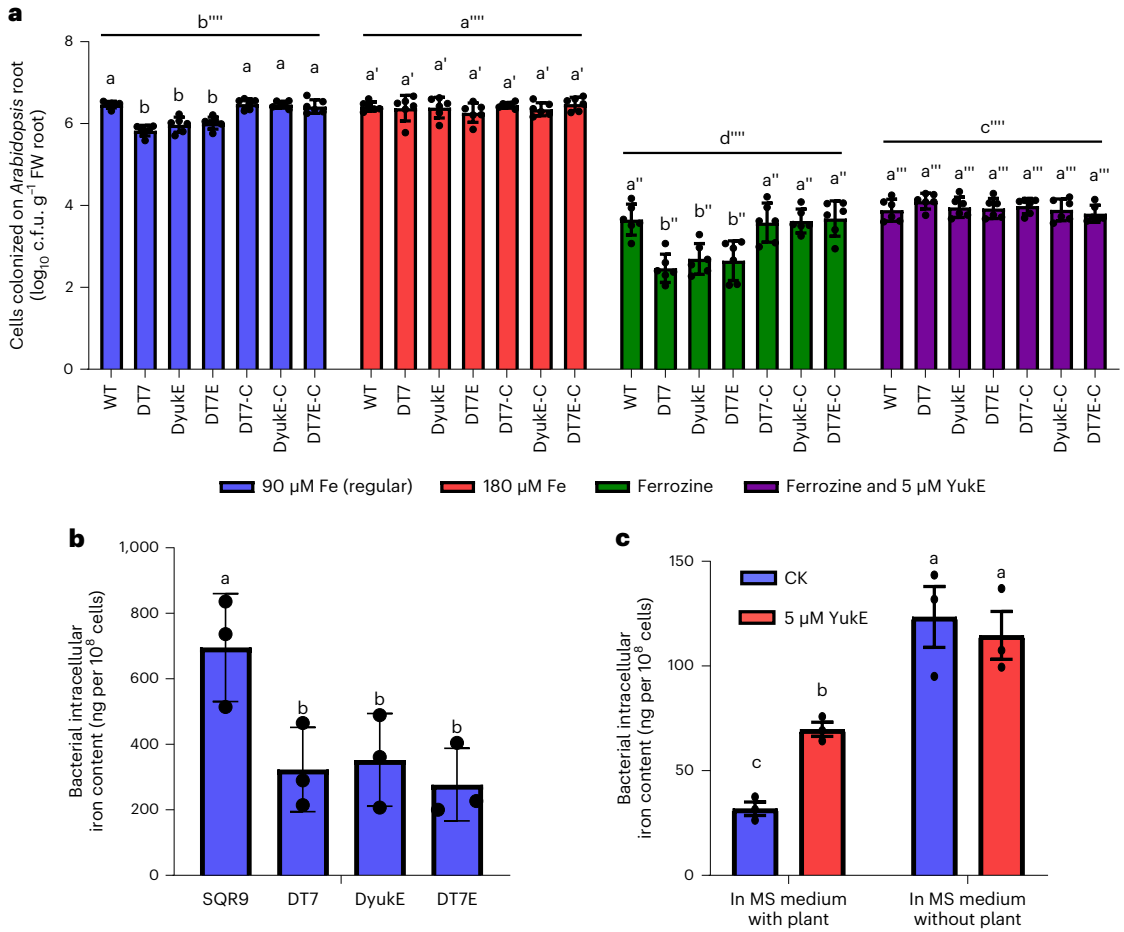

Fig. 3 | YukE-mediated root iron leakage contributes to root colonization by SQR9. a, Colonization at 2 d post-inoculation by *B. velezensis* SQR9 on 15-day-old *Arabidopsis* roots under hydroponic conditions. *Arabidopsis* was grown in iron-free MS medium and was manually supplied with $FeSO_4$. Ferrozine at a final concentration of 300 μM was supplied to generate iron-deprived conditions. The final concentration of 90 μM iron represents the original MS medium. YukE was supplied at a final concentration of 5 μM. Data are presented as mean ± s.e.m. Significant differences were determined with two-sided one-way ANOVA and Duncan's post-hoc test ($n = 6$, $\alpha = 0.05$, $P < 0.001$). The experiment was performed twice and showed similar results. **b**, ICP–MS measurement of the iron acquired by bacterial cells in the rhizosphere of 15-day-old *Arabidopsis* at 24 h post-inoculation. Wild-type SQR9 or the mutants were inoculated into medium-grown 15-day-old *Arabidopsis* plants with regular iron (90 μM). The bacterial cells were collected by vigorous washing and centrifugation at 0 h and 24 h post-inoculation, respectively. Bacterial iron acquisition was calculated as the iron content at 24 h post-inoculation minus that at 0 h post-inoculation. The data were normalized by total cell numbers. Data are presented as mean ± s.e.m. Significant differences were determined with two-sided one-way ANOVA and Duncan's post-hoc test ($n = 3$, $\alpha = 0.05$, $P < 0.001$). This experiment was conducted three times with similar results. **c**, ICP–MS measurement of the iron content of bacterial cells in vitro. Fifteen-day-old *Arabidopsis* plants were treated with 5 μM YukE for 12 h for iron leakage. Untreated plants were included as controls. The plant was removed and the resultant medium was used to culture WT SQR9. Direct culturing of SQR9 with YukE in MS medium for 3 h was included as a negative control. Intracellular iron content was measured by ICP–MS after culturing for 3 h. The data were normalized by total cell numbers. Data are presented as mean ± s.e.m. Significant differences were determined with two-sided one-way ANOVA and Duncan's post-hoc test ($n = 3$, $\alpha = 0.05$, $P < 0.001$). This experiment was conducted three times with similar results.

root iron content is not due to potential contamination during purification. In the shoot, the iron content in response to treatment with WT and mutant SQR9 or that between the untreated control and YukE treatment was not changed or was very mildly changed (Supplementary Fig. 10). In addition, at 48 h and 72 h post-inoculation, neither WT *B. velezensis* SQR9 nor these mutants affected the root iron content (Fig. 2f, and Supplementary Figs. 9 and 10), suggesting that the decrease in root iron content caused by *B. velezensis* SQR9 and YukE occurred only in the early stage of root colonization. We then treated *Arabidopsis* with gradient concentrations of YukE and found that YukE decreased the root iron content at the lowest tested concentration of 1 μM (Fig. 2g). To test whether these root iron-decreasing effects of SQR9 and YukE are consistent under natural conditions, we then grew *Arabidopsis* in sterile soil, sterile soil with the microbial community extracted from natural soil, and natural soil. We also grew cucumber in natural soil and in hydroponic conditions. As expected, WT SQR9 and purified YukE decreased the iron content in the roots of *Arabidopsis* and cucumber in soil-grown conditions, while D7, DyukE and DT7E and YukE^{S38C} did not. The complementary strains decreased the iron content as did WT SQR9 (Supplementary Fig. 11).

K252a, a general kinase inhibitor blocking the potential YukE-sensing process of plants, and brefeldin A (BFA), a general inhibitor of exocytosis in plant cells, were applied individually to determine whether they block the decrease in plant iron content caused by YukE. The Perls staining results showed that the iron-decreasing effect of YukE could only be observed at the root maturation zone (Fig. 2h). The results also showed that neither K252a nor BFA affected the plant iron content, and the iron-decreasing effect of YukE was not compromised in the presence of K252a or BFA (Fig. 2h,i). These results suggest that YukE may decrease the root iron content in a direct way.

https://doi.org/10.1038/s41564-023-01402-1

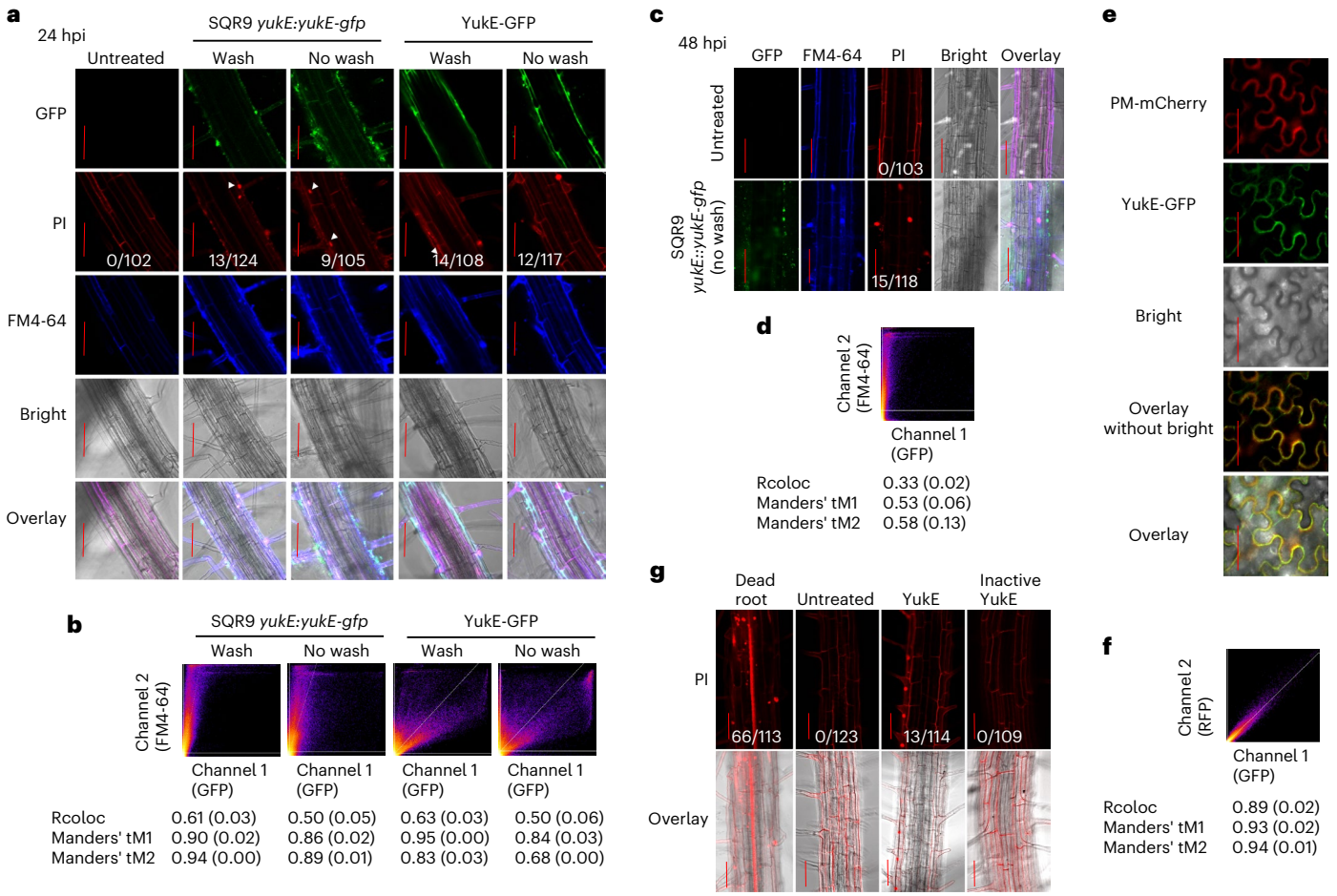

Fig. 4 | YukE function and location on the surface of 15-day-old *Arabidopsis* cells. a, Location of YukE on the root surface at 24 h post-inoculation or treatment. *Arabidopsis* roots were inoculated with *B. velezensis* SQR9 *yukE::yukE-gfp* at a final concentration of 10^7 cells per ml or treated with purified YukE-GFP at a final concentration of 5 μM. The vigorous washing step of the roots was included to remove unattached bacterial cells and proteins. White arrowheads point to nuclei stained by PI. The fraction under each image indicates the number of times the cell nuclei were stained with PI. For each treatment, the maturation zones of 12 roots were examined and showed similar results. Scale bar, 100 μm. This experiment was repeated four times with similar results. **b**, Co-localization analysis of the GFP and FM4-64 signals shown in **a**. Numbers in brackets indicate standard error calculated from all replicates in **a**. **c**, Location of YukE on the root surface at 48 h post-inoculation. Scale bar, 100 μm. **d**, Co-localization analysis of the GFP and FM4-64 signals shown in **c**. The fraction under each image indicates the number of times the cell nuclei were stained with PI. Numbers in brackets indicate standard error calculated from all replicates in **c**. **e**, Co-localization of YukE-GFP and the plasma membrane marker PM-mCherry in *N. benthamiana* leaf cells at 2 d post-inoculation. Three biological replicates were included. Scale bar, 100 μm. This experiment was repeated twice with similar results. **f**, Co-localization analysis of the GFP and the RFP signals shown in **e**. Numbers in brackets indicate standard error calculated from all replicates in **e**. **g**, Effect of YukE on the staining of root cell nuclei by PI. The fraction under each image indicates the number of times the cell nuclei were stained with PI. For each treatment, the maturation zone of 12 roots was examined. Scale bar, 100 μm. This experiment was repeated three times with similar results.

Excess iron rescues the colonization defect of the T7SS mutants

We hypothesized that *B. velezensis* SQR9 may use T7SS-secreted YukE to compete for iron to facilitate its colonization. Thus, a root colonization assay was performed with modified Murashige and Skoog (MS) medium containing a 2-fold higher iron concentration (180 μM Fe). As expected, in the iron-rich MS medium, DT7, DyukE and DT7E did not show differences in root colonization, while in the standard MS medium (90 μM Fe), DT7, DyukE and DT7E all showed significantly lower root colonization (Fig. 3a), indicating that excess iron rescued the root colonization defect of these mutants. In parallel, colonization of *Arabidopsis* roots by WT *B. velezensis* SQR9 was tested in iron-deprived MS medium containing 300 μM ferrozine. Both WT *B. velezensis* SQR9 and the T7SS mutants showed dramatically reduced root colonization in this iron-deprived medium. Moreover, iron limitation amplified the colonization defect of the T7SS mutants compared with that of WT *B. velezensis* SQR9, and the deficiency of colonization of the mutants could also be restored by complementation with the T7SS cluster and *yukE* (Fig. 3a). This experiment was also performed with *Arabidopsis* grown in natural soil and got similar results (Extended Data Fig. 1d). In addition, supplementation of the growth medium with exogenous YukE protein (5 μM) completely rescued the root colonization defect of DT7, DyukE and DT7E in iron-deprived MS medium (Fig. 3a). These results support the hypothesis that YukE contributes to plant root iron leakage to benefit *B. velezensis* SQR9 colonization.

To exclude the possibility that the rescued phenotype may be caused by changes in the growth or biofilm formation of the *B. velezensis* SQR9 T7SS mutants under low- or high-iron conditions, we evaluated the growth and biofilm formation of DT7, DyukE, DT7E and WT *B. velezensis* SQR9 in medium with different iron concentrations. These results showed that excess iron (100 μM) in MSgg medium enhanced biofilm formation, while low iron reduced biofilm formation in all these strains. However, no differences were observed between different strains at the same iron concentration (Supplementary Fig. 12). Moreover, differences in the iron concentration did not influence the

https://doi.org/10.1038/s41564-023-01402-1

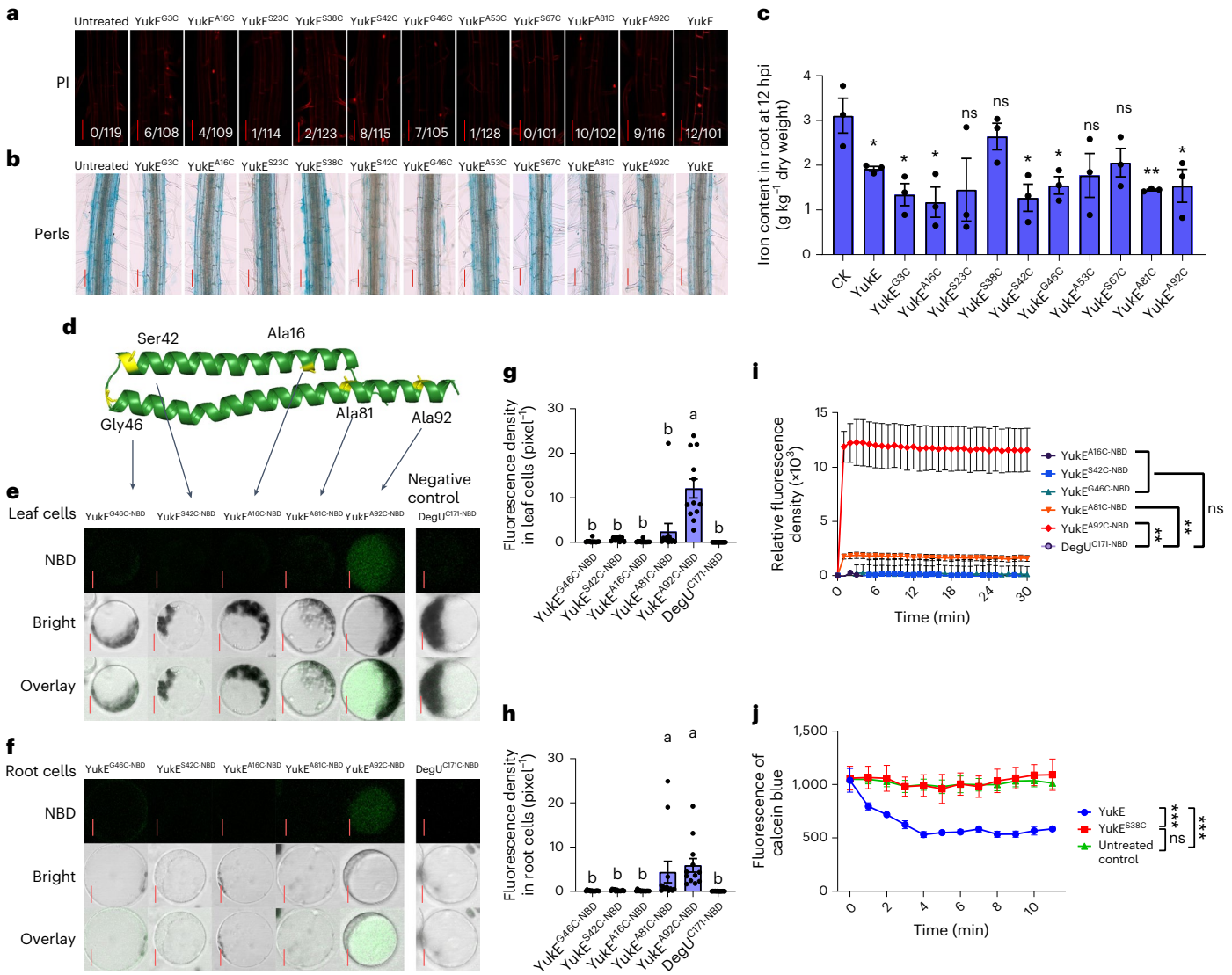

Fig. 5 | Insertion of YukE into the plant plasma membrane. a,**b**, Effect of YukE variants on the staining of root cell nuclei by PI (**a**) and on Perls' staining of iron (**b**) at 24 h post-inoculation. The fraction under each image indicates the number of times the cell nuclei were stained with PI. Scale bar, 100 µm. Blue staining represents iron. **c**, ICP–OES measurement of the iron content in roots of 15-day-old *Arabidopsis* treated with YukE variants at 12 h post-inoculation. CK indicates the untreated plant. Data are presented as mean ± s.e.m. ($n = 3$). *P* values for pairwise two-sided *t*-test are (from left to right): $P = 0.045$, $P = 0.013$, $P = 0.010$, $P = 0.064$, $P = 0.200$, $P = 0.011$, $P = 0.019$, $P = 0.051$, $P = 0.054$, $P = 0.002$, $P = 0.022$. These experiments (**a**–**c**) were repeated twice with similar results. **d**, 3D structure of YukE predicted by AlphaFold 2. The residues coloured yellow indicate the sites labelled with NBD for testing plasma membrane insertion. **e**,**f**, Fluorescence confocal microscopy detected membrane insertion of YukE on leaf (**e**) or root (**f**) protoplasts. Images were taken at 15 h post-mixing. Three replicates were included for each treatment. Scale bar, 20 µm. This experiment was repeated twice with similar results. **g**,**h**, Quantitative analysis of the microscopic view in **e** (**g**) and **f** (**h**). For each cell, the integrated fluorescence density was recorded and normalized by pixel counts. Data are presented as mean ± s.e.m. ($n = 10$). Significant differences were determined with two-sided one-way ANOVA and Duncan's post-hoc test ($n = 3$, $\alpha = 0.05$, $P < 0.001$ for **g**,**h**). **i**, Quantitative analysis of the insertion on artificial liposomes by NBD-labelled YukE variants. Data are presented as mean ± s.e.m. ($n = 3$). *P* values for pairwise two-sided *t*-tests are (from top to bottom): $P = 0.715$, $P = 0.002$ and $P = 0.004$. This experiment was repeated twice with similar results. **j**, Quantitative analysis of the iron released from liposomes. Data are presented as mean ± s.e.m. ($n = 5$). *P* values for pairwise two-sided *t*-tests are (from top to bottom): $P = 8.59 \times 10^{-4}$, $P = 0.1615$ and $P = 2.13 \times 10^{-5}$. This experiment was conducted twice with similar results.

growth of these strains in MSgg medium (Supplementary Fig. 13), and excess YukE protein had no effect on the growth and biofilm formation of these strains (Supplementary Figs. 14 and 15).

We then hypothesized that YukE-induced root iron leakage may affect bacterial iron homoeostasis and therefore influence bacterial colonization. We quantitatively measured the iron acquired by the bacterial cells after inoculation into the *Arabidopsis* rhizosphere by ICP–MS. As expected, WT SQR9 acquired 2-fold more iron in the rhizosphere than DT7, DyukE and DT7E (Fig. 3b), while WT SQR9 showed the same iron acquisition efficiency as DT7, DyukE and DT7E in Luria-Bertani (LB) medium (Supplementary Fig. 16). To further confirm whether YukE-induced iron leakage leads to this difference, the plant was treated with YukE, then the plant was removed and the resultant medium was used to culture SQR9. The iron content of SQR9 cells was measured by ICP–MS. The results showed that YukE-treated *Arabidopsis* medium increased the cellular iron content of SQR9 (Fig. 3c). In addition, YukE did not increase the iron content of SQR9 cells in medium without plant roots (Fig. 3c). These results suggest that root iron leakage caused by T7SS and YukE increased the iron content of SQR9.

https://doi.org/10.1038/s41564-023-01402-1

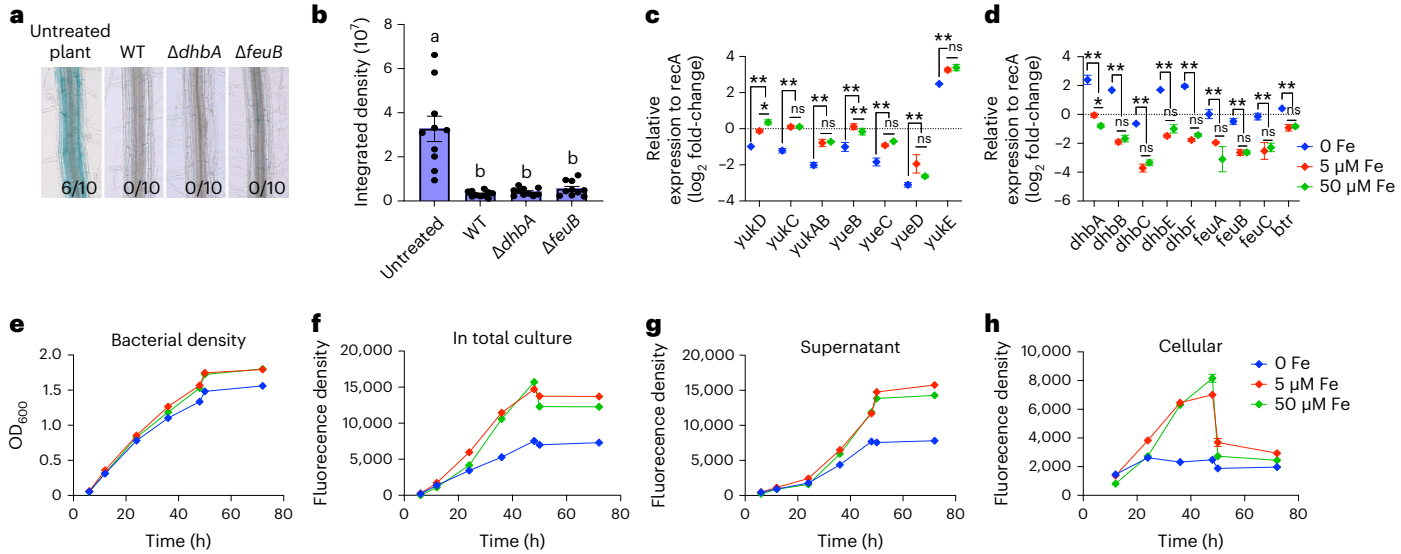

Fig. 6 | Comparison of the function of the T7SS and the siderophore-Feu system in *B. velezensis* SQR9. **a**, Microscopic view of Perls staining of the root iron content. Fifteen-day-old *Arabidopsis* was inoculated with *B. velezensis* and the siderophore- or Feu-deficient mutant. Images were taken at 24 h post-inoculation. Blue staining represents iron. For each treatment, the maturation zone of 10 roots was examined. Scale bar, 100 μm. The fraction under each image indicates the number of times root staining occurred (with more than 300,000 blue pixels in 1.5 mm root) relative to the number of examined images. This experiment was repeated twice with similar results. **b**, Quantitative analysis of the microscopic view of Perls staining in **a**. Data are presented as mean ± s.e.m. Significant differences were determined with two-sided one-way ANOVA and Duncan's post-hoc test ($n = 10$, $\alpha = 0.05$, $P < 0.001$). **c**,**d**, qRT–PCR for measuring the expression of genes in the T7SS (**c**) and the siderophore-dependent iron acquisition strategy (**d**) at 8 h post-treatment. The expression of *recA* was used as an internal reference. Data are presented as mean ± s.e.m. ($n = 3$). *P* values for pairwise two-sided *t*-test are (from left to right): (**c**) $P = 5.6 \times 10^{-4}$, $P = 0.013$, $P = 3.86 \times 10^{-8}$, $P = 0.872$, $P = 2.16 \times 10^{-6}$, $P = 0.639$, $P = 2.45 \times 10^{-4}$, $P = 4.27 \times 10^{-5}$, $P = 1.16 \times 10^{-5}$, $P = 0.125$, $P = 0.028$, $P = 0.081$, $P = 3.35 \times 10^{-5}$, $P = 0.342$; (**d**) $P = 9.52 \times 10^{-5}$, $P = 0.021$, $P = 1.10 \times 10^{-7}$, $P = 0.199$, $P = 7.02 \times 10^{-7}$, $P = 0.119$, $P = 1.64 \times 10^{-6}$, $P = 0.161$, $P = 1.98 \times 10^{-8}$, $P = 0.102$, $P = 0.002$, $P = 0.105$, $P = 1.99 \times 10^{-7}$, $P = 0.963$, $P = 5.56 \times 10^{-5}$, $P = 0.550$, $P = 3.96 \times 10^{-6}$, $P = 0.557$. This experiment was conducted three times with similar results. **e**–**h**, Effect of iron conditions on YukE secretion by *B. velezensis* SQR9. **e**, Bacterial density recorded at OD_{600}. **f**, YukE production was recorded as the fluorescence density of the total culture. **g**, YukE secretion from cells recorded as the fluorescence density of the supernatant of the culture. **h**, YukE in cells recorded as the fluorescence density of the lysate of bacterial cells. Data are presented as mean ± s.e.m. ($n = 3$). These experiments (**e**–**h**) were repeated twice with similar results.

We wondered whether YukE is disadvantageous to plant growth. Interestingly, we found that the application of YukE alone did not affect plant growth, but significantly enhanced the growth-promoting effect of *B. velezensis* SQR9 on cucumber (Extended Data Fig. 3). This result indicates that the YukE-mediated root iron decrease was temporary and did not negatively affect plant growth, which is in line with the fact that the decrease in iron content was no longer observed at 48 h.

YukE inserts into the root cell membrane and causes iron leakage

The *M. tuberculosis* T7SS cargo protein EsxA, which is homologous and structurally similar to YukE[21], has been reported to be inserted into the host membrane to form a pore, causing leakage of the phagolysosome[18,39]. We wondered whether YukE may reduce the plant root iron content by direct insertion into the root cell membrane to cause iron leakage. *B. velezensis* SQR9 *yukE::yukE-gfp* was used to observe the location of YukE on plant roots. Propidium iodide (PI) and *N*-(3-triethylammoniumpropyl)-4-(6-(4-(diethylamino) phenyl) hexatrienyl)pyridinium dibromide (FM4-64) were used simultaneously to stain the plasma membrane of roots. At 24 h post-inoculation with SQR9 *yukE::yukE-gfp*, YukE was detected at the root surface (Fig. 4a,b). Treatment with purified YukE-GFP also revealed its location on the root surface (Fig. 4a,b). Vigorous washing of the SQR9 *yukE::yukE-gfp*-inoculated or YukE-GFP-treated roots removed the majority of the SQR9 cells but not the GFP signals (Supplementary Fig. 17), suggesting that the secreted YukE and purified YukE remain attached to the roots. At 48 h post-inoculation of SQR9 *yukE::yukE-gfp*, less YukE was detected on the root surface (Fig. 4c,d). This may explain the fact that the SQR9 YukE-mediated decrease in root iron content is transient and no longer detectable at 48 h post-inoculation.

To confirm whether YukE functions in the plant cell membrane, YukE-GFP was expressed in *N. benthamiana* cells by using an *Agrobacterium*-mediated transient expression assay. A plasma membrane marker (PM-mCherry) showed an association of YukE-GFP with the plasma membrane (Fig. 4e,f). To confirm whether YukE changed the root cell membrane structure, YukE-, YukE-GFP- or *B. velezensis* SQR9 *yukE::yukE-gfp*-treated plant roots were stained with the general dye PI. Results showed that the cell nuclei of YukE-treated roots, but not untreated roots, could be stained by PI (Fig. 4a,g). PI can stain plant cell nuclei only when the plant cell membrane permeability is changed. In addition, YukE did not cause the death of plant root cells, as observed by microscopy (Fig. 4g).

To further confirm the function of YukE in plant cell membrane permeability and root iron leakage, we generated and purified several YukE variants with mutations at a single site to test their functions (Supplementary Fig. 5g). The mutation sites were chosen to spread over the entire sequence. We found that YukE mutations of S23C, S38C, A53C and S67C, but not G3C, A16C, S42C, G46C, A81C and A92C, caused loss of function in both changing membrane permeability and causing iron leakage (Fig. 5a–c), which provides further evidence of YukE function.

NBD (*N*,*N*′-dimethyl-*N*-(iodoacetyl)-*N*′-(7-nitrobenz-2-oxa-1,3-diazol)ethylenediamine), a dye that emits strong fluorescence when inserted into lipid membranes using as a fluorescence marker for protein membrane insertion, was then used to label the Cys residue of the YukE variants, which maintained the ability to cause root iron leakage[18,39]. Each of the NBD-labelled YukE variants (YukE-NBD) was co-incubated with root or leaf protoplasts to test the plasma membrane insertion of each position of the protein (Fig. 5d). $YukE^{A92C\text{-}NBD}$ showed strong fluorescence when co-incubated with either leaf or root protoplasts in comparison with $DegU^{C171\text{-}NBD}$, which served as a

negative control (Fig. 5e–h). We also co-incubated each YukE-NBD with artificial liposomes and found that YukE$^{A92C\text{-}NBD}$ treatment showed strong and significant fluorescence, while YukE$^{A81C\text{-}NBD}$ showed mild but still significant fluorescence in comparison with the negative control (Fig. 5i). Because the fluorescence density of NBD is positively correlated with the environmental hydrophobicity, we concluded that YukE could insert into the plasma membrane and that the A92 position was nearer to the center of the phospholipid bilayer.

We then wondered whether the membrane insertion of YukE is directly relevant to iron leakage. Thus, liposomes encapsulating iron were treated with YukE and the released iron was measured. As expected, YukE caused iron leakage from the liposome, while YukE^{S38C} did not (Fig. 5j), indicating that YukE caused iron release across the liposome membrane. These results conclusively support the hypothesis that YukE directly inserts into root cell membranes to cause root iron leakage (Extended Data Fig. 4).

We wondered whether any other ions besides iron, such as potassium and calcium, would leak from root cells when roots were treated with YukE or live SQR9. Results showed that the potassium and calcium contents in roots and shoots were not or were very mildly decreased when the roots were treated with YukE or inoculated with SQR9. No significant differences were observed between treatments of WT SQR9, DT7, DyukE or DT7E (Supplementary Figs. 18 and 19).

Division of labour between T7SS and siderophore strategy

Siderophore-dependent iron acquisition is an important strategy by which bacteria acquire environmental iron. *B. velezensis* SQR9 produces bacillibactin (BB) as a siderophore to bind iron in the environment, and BB-bound iron is then transported into bacterial cells by FeuABC[12]. To distinguish the function of T7SS and siderophore-dependent iron acquisition, *B. velezensis* SQR9 mutants with BB or FeuA deficiency were obtained, but they did not compromise the ability to decrease the root iron content (Fig. 6a,b). These results indicate that the BB-Feu system did not contribute to plant root iron leakage. Therefore, the T7SS function and siderophore-dependent iron acquisition systems should have a clear division of labour—while siderophores function in a low-iron environment to compete for iron with other microbes, the T7SS represents a strategy by which rhizosphere *Bacillus* species temporarily cause iron leakage from the host for fast occupancy of niches. We then evaluated how their expression was affected by the environmental iron level. The results showed that T7SS expression under high levels of iron (5 μM and 50 μM) was significantly higher than that under low levels of iron (0 Fe) (Fig. 6c), while in the siderophore strategy, the transcriptional regulator Btr and the downstream BB synthetase (Dhb) and transporter (Feu) genes were induced under low levels of iron (Fig. 6d). The intracellular or extracellular levels of YukE were consistent with the RT–qPCR results (Fig. 6e–h). The finding also suggests that YukE secretion by *B. velezensis* and the decrease in root iron content is in a positive feedback loop. When root iron leakage occurred, the secretion and production of YukE in *B. velezensis* SQR9 were induced, which caused more root iron leakage (Extended Data Fig. 5).

Discussion

Since the T7SS was discovered in *Bacillus*, its biological and ecological significance has never been revealed. In the present study, we revealed that *Bacillus* T7SS and the secreted protein YukE facilitated root colonization by the beneficial rhizobacterium *B. velezensis* SQR9 by causing root iron leakage in the early colonization stage. We further confirmed that YukE caused changes in root cell membrane permeability by directly inserting into the root plasma membrane (Extended Data Fig. 4). We illustrated the possible regulation of T7SS by iron (Extended Data Fig. 5).

In *Bacillus*, YukE is homologous to EsxA, a WXG100 family protein in the tuberculosis-causing pathogen *M. tuberculosis*[19–21]. EsxA plays an essential role in phagosome rupture and bacterial cytosolic translocation within host macrophages[40]. In vitro experiments showed that EsxA is inserted into the lysosome membrane and has membranolytic activity, which contributes to lysosome lysis by *M. tuberculosis*, thereby helping the invasion of this pathogen from lysosomes into the cytoplasm of macrophages[16,18,39]. However, the membranolytic activity of EsxA at neutral pH was reported to potentially be ascribed to detergent contamination in the purification of EsxA[41,16]. Deletion of the gene encoding an essential component of the T7SS from *S. aureus* RN6390 was found to cause an iron starvation response in the bacterium and its T7SS was found to be transcriptionally regulated by iron[42]. Here we propose that YukE causes root cell iron leakage by inserting into root membrane. The structure of YukE shows no membrane-spanning region. The YukE homodimer, which was built on the basis of the EsxA model of *M. tuberculosis*, shows enriched hydrophobic residues between the 4 helixes (Extended Data Fig. 6a–c). We hypothesize that YukE might have a changed structure when present in the plasma membrane that exposes the hydrophobic side out. Based on structure comparison, we found that the crystal form of *Geobacillus thermodenitrificans* EsxA (PDB identifier: 3ZBH), which is homologous to YukE (56.7% identity), is in an asymmetric unit including four homodimers. The asymmetric unit forms a pore-like structure in a side-by-side manner (Extended Data Fig. 6d–f). This structure suggests that YukE homodimers could potentially form an advanced structure bound with their hydrophilic side to each other and thus expose the hydrophobic side out. In the interaction between macrophages and *Legionella pneumophila*, a function of the type IV secretion system (T4SS) similar to that of the T7SS shown in this study was reported[43]. A T4SS-secreted protein, MavN, was found to be inserted into host membranes to mediate iron acquisition[43].

Plant pathogens use diverse strategies to obtain iron from plants[10,11], but beneficial bacteria have not been considered to decrease plant iron content. The T7SS is highly conserved in beneficial plant *Bacillus* strains. Hence, the root iron-decreasing effect in the early colonization stage is likely to generally occur during ubiquitous plant–*Bacillus* interactions. As shown above and in a previous study, a reactive oxygen species burst takes place during the very early stage of root colonization by *B. velezensis*[24]. Reactive oxygen species can react with cytoplasmic iron through the Fenton reaction to produce hydroxyl radicals (·OH), which are deleterious to cells[44]. In contrast, iron is an important factor for the colonization of *B. velezensis*[12]. Therefore, root iron leakage in the early colonization stage may benefit both plants and rhizobacteria.

The iron-decreasing effect was observed only in the first 24 h (Fig. 2d,e and Supplementary Fig. 9); at 48 h post-inoculation, all treatments with *B. velezensis* SQR9 or the mutants had no effect on root iron content in comparison with untreated plants (Fig. 3f and Supplementary Fig. 10). Moreover, YukE alone did not show a negative effect on plant growth and it even enhanced the growth-promoting effect of *B. velezensis* SQR9 (Extended Data Fig. 3). These results indicated that YukE is beneficial to *Bacillus* colonization and to the plant growth-promoting effect, in contrast to the unilateral effect of effectors from pathogenic bacteria[45]. However, the termination mechanism of root iron leakage was not elucidated in this study.

Overall, in this study, we revealed that the T7SS of *B. velezensis* SQR9 and its secreted protein YukE cause iron leakage in plant roots, which promotes root colonization by *B. velezensis* SQR9.

Perspectives

Further investigation may reveal deeper interaction mechanisms between bacterial T7SS and plant roots. How is the leakage terminated after the early stage of colonization? Moreover, it is necessary to determine other possible components that leak from root cells in response to YukE. How does *Bacillus* remain the first beneficiary of root-leaked iron in a complex soil environment? Answering these questions will greatly expand our knowledge of the interaction between plant roots and rhizobacteria.

Methods

Experimental materials

Arabidopsis thaliana accession Col-0 was used in this study. For experiments conducted under hydroponic conditions, *Arabidopsis* seeds were surface sterilized with 2% (v/v) NaClO. The sterile seeds were placed in Petri dishes containing 1/2 MS medium with 2% (w/v) sucrose and 0.8% (w/v) agar, and vernalized for 2 d at 4 °C in darkness. Then, seeds on Petri dishes were cultured under 16 h light and 8 h dark cycles at 22 °C for 1 week, and the seedlings were then transferred to new Petri dishes containing 1/2 MS medium with 0.5% (w/v) sucrose and 1.5% (w/v) agar, or 6-well plates containing liquid 1/2 MS medium with 0.5% (w/v) sucrose and cultured for one more week for experimental use.

For experiments conducted under soil conditions, *Arabidopsis* seedlings were cultivated in a sterile FlowPot device (Extended data Fig. 1a) as previously described[46]. Soil was collected from the Hulunber Grassland Ecosystem Observation and Research Station located at the Xiertala farm, Inner Mongolia, China (49.414° N, 120.078° E; pH, 6.07 ± 0.09; organic matter, 29.47 ± 0.81 g kg^{-1}). Sterile soil was prepared by double autoclaving at 121 °C for 30 min with a 48 h interval. To prepare the sterile soil with the extracted microbial community as previously described[46], the natural soil was incubated at room temperature for 1 week with ~50% relative humidity before the extraction of the microbial community. Then, 425 ml of distilled water and 25 g of the soil were added to a 1 l flask, which was shaken for 20 min and then allowed to stand for 5 min, allowing the large particles to settle down. The suspension was filtered through a 70 μm cell strainer (Celltreat Scientific, 229483); the soil slurry was then mixed with sterile 1× LS medium[46] and inoculated into the sterile soil. The syringe in FlowPot was filled with natural soil, autoclaved soil, or autoclaved soil inoculated with the extracted microbial community. A sterile Luer–female Luer adapter was attached to another sterile 50 ml syringe, which was used to infiltrate each FlowPot with inoculant. *Arabidopsis* seeds were sown in the FlowPot and allowed to grow at 22 °C in a growth chamber with a 16 h light/8 h dark photoperiod. Fifteen-day-old *Arabidopsis* seedlings were used for further treatment.

The 'Chinese long' cucumber inbred line 9930 was used in this study. The cucumber seeds were surface sterilized with 75% (v/v) ethanol and then with 2% (v/v) NaClO. The seeds were planted into culture bottles containing vermiculite and allowed to germinate and grow for 4 d in a growth chamber at 28 °C with a 16 h light and 8 h dark photoperiod. For the experiment conducted under hydroponic conditions, the seedlings were then transplanted into 50 ml flasks (one seedling per flask) containing 35 ml of sterile liquid (sucrose-free 1/2 MS medium) to submerge the seedling roots in the medium, and cultured for 3 weeks with gentle shaking (50 r.p.m.) for 2 h each day on a shaker. The MS medium was replaced every other day during the growth period. For the experiment conducted in soil (similar to the soil used for growing *Arabidopsis*), the germinated cucumber seedlings were transferred to square pots containing natural soil and allowed to grow in a growth chamber at 28 °C with a 16 h light and 8 h dark photoperiod. Cucumber seedlings at 21 d post-germination were used for further treatment.

B. velezensis SQR9 (China General Microbiology Culture Collection Center, CGMCC accession number 5808) and the derived strains were grown at 30 °C on LB medium (10 g l^{-1} peptone, 5 g l^{-1} yeast extract and 5 g l^{-1} NaCl) agar plates. MSgg medium (5 mM potassium phosphate (pH 7), 100 mM 3-(*N*-morpholino)propanesulfonic acid (pH 7), 2 μM $MgCl_2$, 700 μM $CaCl_2$, 50 μM $MnCl_2$, 50 μM $FeCl_3$, 1 μM $ZnCl_2$, 2 μM thiamine, 0.5% glycerol, 0.5% glutamate, 50 μg ml^{-1} tryptophan and 50 μg ml^{-1} phenylalanine) was used for biofilm formation[28]. When necessary, antibiotics were added at the following final concentrations: chloramphenicol at 5 mg l^{-1}, zeocin at 20 mg l^{-1}, spectinomycin at 100 mg l^{-1}, rifampicin at 50 mg l^{-1}, erythromycin at 1 mg l^{-1} and kanamycin at 30 mg l^{-1}. Information on the strains used in this study is provided in Supplementary Table 4.

Genetic assay for *B. velezensis*

Gene deletion mutants were constructed using unmarked genetic manipulation based on multiple gene deletions by relying on a counter-selectable marker, *pheS*[47]. All these mutants were verified by PCR and sequencing. Complementary strains of these mutants were constructed by transforming a plasmid pNW33n carrying deleted genes with their original promoters into the corresponding mutants. A *gfp* gene fragment was introduced into the genome of WT SQR9 and the derived strains for qPCR detection in soil. YukE was also labelled with GFP at the C terminus in vivo to generate SQR9/*yukE::yukE-gfp* and DT7/*yukE:yukE:gfp*. The plasmid pNW33n carrying the gene encoding mVENEUS was introduced into SQR9/*yukE::yukE-gfp*. Essential antibiotic resistance genes were included as selectable markers. Detailed information on the strains used is provided in Supplementary Table 4 and information on the primers used for genetic manipulation is provided in Supplementary Table 5.

Root colonization assay

To measure the colonization of *Arabidopsis* roots grown under hydroponic conditions, 7-day-old *Arabidopsis* Col-0 plants were transferred from 1/2 MS agar plates to 6-well plates containing liquid 1/2 MS with 0.5% sucrose (3 seedlings per well). After 7 d, the medium was replaced with differentially modified 1/2 MS medium without sucrose and $FeSO_4$ for the experiment. Generally, the MS medium without sucrose and Fe used in the colonization period was modified to include 300 μM ferrozine, 90 μM $FeSO_4$ or 180 μM $FeSO_4$ to generate an iron concentration gradient. Ferrozine has high affinity for iron and was used to capture iron, thereby producing iron-deficient conditions. For the experiment with YukE, the purified YukE protein was added to the rhizosphere at a final concentration of 5 μM. WT *B. velezensis* SQR9, the mutated strains and the complementary strains were inoculated into each well at a final concentration of 10^7 cells per ml. The root samples were collected at 2 d after treatment and washed three times with water. The samples were placed in 2 ml tubes containing 3 zirconium beads, weighed and suspended in 1 ml 0.1 M PBS using a Mixer Mill MM400 (Retsch) with a frequency of 30 beats per second. To measure the colonization of cucumber roots grown under hydroponic conditions, 21-day-old cucumber seedlings were used for inoculation. WT *B. velezensis* SQR9 and the mutated strains were inoculated at a final concentration of 10^7 cells per ml. Roots were sampled at 2 d after inoculation. The colonized cells were collected by maximum vortexing of the roots. Bacterial densities were assessed by plating dilutions of the samples onto LB agar medium. The plates were incubated at 30 °C for 12 h and then, the numbers of colony forming units (c.f.u.s) were determined. Each treatment included 6 replicates.

To measure the colonization of *Arabidopsis* roots grown in soil conditions, seedlings grown in FlowPots were inoculated with gfp-labelled SQR9 or the derived strains at a final concentration of 10^7 cells per ml. In addition, 300 μM ferrozine or 180 μM $FeSO_4$ was added together with the inoculant when necessary. At 2 d post-inoculation, the rhizosphere soils of plants were collected for DNA extraction as previously described[48]. To measure the colonization of cucumber roots grown in soil conditions, 21-day-old seedlings were inoculated with gfp-labelled SQR9 or the derived strains at a final concentration of 10^7 cells per ml. After 2 d of inoculation, the rhizosphere soils of plants were collected for DNA extraction. Quantification of gfp-labelled SQR9 and the derived strains was performed using qPCR and normalized to root fresh weight as described previously[49].

Biofilm formation assay

The biofilm formation assay was performed as previously described[28]. *B. velezensis* SQR9 and its derived mutants were cultured in LB medium until the optical density $(OD)_{600}$ reached 1.0. The bacterial cells were collected by centrifugation at 6,000 *g*. The pellets were washed with sterile water three times and suspended in MSgg medium at an OD_{600}

of 1.0. Biofilms were formed in 48-well microtitre plates. Each well was filled with 1 ml of MSgg medium inoculated with a 10 µl suspension of *B. velezensis* SQR9 or the derived mutants. The negative control contained only the corresponding culture medium. For biofilm formation under unique conditions, such as in iron-free, low-iron and YukE-containing media, the final concentration used was the same as that in the colonization experiment. Every biofilm formation condition included 4 replicates.

Motility assay

The swarming assay was performed following a previously described method[50]. Briefly, *B. velezensis* SQR9 and its derived mutants were cultured in LB medium until the OD_{600} reached 0.8. The cultures were inoculated on Petri dishes containing semisolid LB medium (0.5% (w/v) glucose and 0.6% (w/v) Eiken agar (Eiken)) using sterilized toothpicks. The Petri dishes were incubated at 37 °C for 4–6 h to allow the bacterial cells to swarm. Then, the water content of the medium in the Petri dishes was reduced with dry air to terminate the swimming process. Subsequently, the Petri dishes were incubated overnight at room temperature. The swarming circles on the Petri dishes were observed and recorded after 24 h. Four replicates were included for each strain.

Protein purification

Exogenous expression and purification of YukE, YukE-GFP and the YukE variants $YukE^{G3C}$, $YukE^{A16C}$, $YukE^{S23C}$, $YukE^{S38C}$, $YukE^{S42C}$, $YukE^{G46C}$, $YukE^{A53C}$, $YukE^{S67C}$, $YukE^{A81C}$ and $YukE^{A92C}$ were performed in an *E. coli* BL21(DE3)/pET29a system. These amino acids were mutated to cysteine to label YukE with the NBD[39]. These sites were selected to cover the entire gene sequence according to the site selection in ref. 39. The DNA fragments encoding the full-length wild-type YukE and GFP were amplified from *B. velezensis* SQR9 genomic DNA or pNW33N-gfp, respectively. Detailed information on the primers used for genetic manipulation is shown in Supplementary Table 5. The PCR products were cloned into the expression plasmid pET29a (+) (Novagen) by a one-step cloning kit (Vazyme Biotech). The reconstructed plasmid was verified by DNA sequencing. The plasmid was introduced into *E. coli* BL21(DE3) for expression. The expressed proteins contained an N-terminal 6His tag. The obtained strains were grown in LB medium at 37 °C with shaking at 200 r.ppm. When the OD_{600} reached 0.5, the growth temperature was lowered to 16 °C. After another 30 min incubation, protein expression was induced by adding 0.03 mM isopropyl-b-D-thiogalactopyranoside. The incubation was continued overnight at 16 °C with shaking at 200 r.p.m. before cell collection by centrifugation at 8,000 × *g* for 10 min. The cell pellets were resuspended and disrupted by sonication (2 s pulse on, 3 s pulse off). The cellular lysates were centrifuged at 20,000 × *g* for 50 min. Finally, for further clarification, the lysates were passed through a 0.22 µm filter (Millipore), followed by purification with His-affinity resin chromatography. The purified proteins were collected and stored in PBS at −80 °C. The N-terminal 6His tag was removed by tobacco etch virus protease (TEV), followed by His-affinity resin chromatography.

Inactivation of YukE by heating

To obtain the negative control for YukE, purified YukE was treated with boiling water bath for 15 min. To compare the heat-treated and original YukE, they were freeze-dried to powder, mixed with KBr powder (1:100 m/v) and ground before analysis by Fourier transform infrared spectroscopy (Nicolet iS10, Thermo Fisher) with a resolution of 8 cm^{-1} between 4,000 cm^{-1} and 400 cm^{-1}. The generated data were analysed by Omnic (v.8.2) and Peakfit (v.4.1.2). The amide I region (1,600–1,700 cm^{-1}) describes C = O stretching in protein structures[51], the amide II region (1,500–1,600 cm^{-1}) describes C = O stretching vibrations and NH bending/CN stretching vibrations[52] and the amide III region (1,200–1,350 cm^{-1}) describes CN stretching and NH bending in protein structures[53]. Four independent replicates were included for each treatment.

Western blot assay

The secretion of YukE-GFP by SQR9 was verified by western blot assay using anti-YukE antibody and anti-RpoD antibody. WT *B. velezensis* SQR9/*yukE-gfp* and DT7/*yukE-gfp* were grown in LB medium for 48 h. The bacterial cells collected from 2 ml culture were resuspended in lysis buffer (0.01 mg ml^{-1} DNase I, 0.1 mg ml^{-1} RNase A, 1 mg ml^{-1} lysozyme, 1 mM phenylmethylsulfonyl fluoride), and the mixture was incubated for 20 min at 37 °C. Glass beads were added and the mixture was vortexed for 2 min. The supernatant of the cell lysate was collected for western blotting. The supernatant of a 2 ml culture was passed through a 0.22 µm filter (Millipore) and the flow-through was treated with an equal volume of 20% (v/v) TCA (Trichloroacetic acid) for 15 h at 4 °C. The precipitate was collected by centrifugation and then washed with precooled acetone three times. The resulting protein sample was used for further analysis by western blotting. The polyclonal anti-YukE and anti-RpoD (as internal control) antibodies were generated by AtaGenix and used at 1:1,000 dilution. HRP goat anti-rabbit IgG was used at 1:10,000 dilution (Abbkine, A21020). Proteins were separated by SDS–PAGE and detected by western blot assay. Purified YukE-GFP and RpoD (as control) were loaded into each lane of an SDS–12.5% polyacrylamide gel. The proteins were transferred to a cellulose nitrate membrane using an SPJ-1000 Atransfer system (Pyxis). The membrane was blocked with 5% skim milk (v/v). Visualization was performed using BeyoECL Moon (Beyotime). The Western blots were scanned by using a ChemiDoc imaging system (Bio-Rad).

Bacterial GFP fluorescence density detection

The fluorescence density was determined for the total culture, supernatant and lysate of *B. velezensis* SQR9/*yukE-gfp* cells to determine the YukE concentration. The standard curve was obtained by detecting the purified YukE-GFP expressed using the pET29a-*E. coli* BL21 protein expression system. The fluorescence density was measured using an Infinite M200 PRO (Tecan) controlled by Tecan i-control software (v.1.12). Six replicates were included.

Bacterial iron content measurement

To measure the iron acquisition of the bacterial cells in the rhizosphere, roots of 15-day-old *Arabidopsis* grown in 6-well plates were inoculated with *B. velezensis* SQR9 or the derived mutants at a final concentration of 10^7 cells per ml. The bacterial cells were collected immediately or at 24 h post-inoculation and washed with deionized water three times. Subsequently, the bacterial cells were centrifuged. To evaluate the iron content of the bacterial cells in the medium, WT SQR9 and the mutant strains were cultured in LB medium, and the cells were collected at 12 h, 24 h and 48 h post-inoculation. The collected bacterial cells from the rhizosphere and medium were digested with HNO_3 at 65 °C for 45 min. The resultant solution was subjected to ICP-MS analysis. The bacterial iron acquisition in the rhizosphere was calculated as the iron content at 24 h post-inoculation minus that at 0 h post-inoculation. The bacterial cells were counted by dilution and plate counting before being subjected to ICP-MS analysis. The cell numbers were used for normalization. Every treatment included 3 replicates.

To evaluate whether YukE-treated plants increased bacterial intracellular iron content, we treated roots of 15-day-old *Arabidopsis* grown in 6-well plates (MS medium) with 5 µM YukE for 12 h and then removed the plants. The resultant medium was used to culture SQR9, and the growth medium of plants without YukE treatment was used as a control to culture SQR9. In parallel, MS medium with YukE was used as a blank control to culture SQR9 and measure the iron content to exclude the possible direct effect of YukE on bacterial iron content. The SQR9 cells were inoculated into these media at a final concentration of 10^7 cells per ml. After 3 h, SQR9 cells were collected and washed with deionized water three times. Subsequently, the bacterial cells were collected and subjected to ICP-MS analysis as described above. Every treatment included 3 replicates.

Bacterial growth measurement

Growth curves of *B. velezensis* SQR9 and the mutant strains in LB medium or under the same conditions as the biofilm formation assay in modified MSgg medium were measured. Measurement of OD_{600} was performed every hour using the Bioscreen C system. Six replicates were included for each treatment.

Plant iron content measurement

For Perls staining, roots of 15-day-old *Arabidopsis* grown in 6-well plates were treated with *B. velezensis* SQR9, its derived mutants and complementary strains, or YukE. *B. velezensis* SQR9 or its derived strains were inoculated at a final concentration of 10^7 cells per ml. YukE or heat-treated YukE was added to the rhizosphere at a final concentration of 5 μM. At 24 h, 48 h and 72 h post-inoculation or treatment, roots were collected for iron content measurement by Perls staining. K252a and brefeldin A (BFA) dissolved in DMSO (dimethyl sulfoxide) were added at final concentrations of 1 μM and 100 μg ml^{-1}, respectively, to evaluate their effect on YukE function. The staining method was as follows: roots were vacuum soaked in Perls staining solution containing 4% (w/v) K-ferrocyanide and 4% (v/v) HCl for 15 min and washed three times with deionized water to terminate the reaction and completely remove the solution[31,54]. The formation of a blue pigment indicates the accumulation of iron. The results were observed and imaged using an Olympus light microscope under a ×10 objective lens. The intensity of the staining was quantitatively analysed using ImageJ (v.1.53). For each image, 1.5 mm roots were selected and the integrated density of blue pixels was calculated (with a density threshold between 59–89 after splitting channels). Each treatment included data from 12 roots from 3 biological replicates.

Iron content measurement was also performed by using inductively coupled plasma–mass spectrometry (ICP-MS) as described previously[12]. For *Arabidopsis* grown in a hydroponic system, roots of 15-day-old *Arabidopsis* grown in 6-well plates were inoculated with WT *B. velezensis* SQR9 or the derived strains, or treated with YukE. WT *B. velezensis* SQR9 or the derived strains were inoculated at a final concentration of 10^7 cells per ml and YukE was added to the rhizosphere at a final concentration of 5 μM. To determine the minimal concentration of YukE needed to modulate root iron content, YukE was added to the rhizosphere at final concentrations of 5 μM, 1 μM, 200 nM, 40 nM, 8 nM and 1.6 nM. Briefly, plant tissues were collected and washed with deionized water three times, and ultrasonic cleaning was performed for 30 s to remove the bacteria on the plant surface and to exclude the bacterial cells and iron contamination from the medium. Subsequently, the tissues were dried at 70 °C for 3 d. For *Arabidopsis* grown in soil, WT *B. velezensis* SQR9 or the derived strains, and YukE or $YukE^{S38C}$ were supplied to FlowPots at final concentrations of 10^7 cells per ml and 5 μM, respectively. The roots were collected carefully and shaken within water and then dried at 70 °C for 3 d. For cucumber grown in a hydroponic system, roots of 21-day-old seedlings were inoculated with WT *B. velezensis* SQR9 or the derived strains at a final concentration of 10^7 cells per ml, or treated with YukE or $YukE^{S38C}$ at a final concentration of 5 μM. The roots were collected at 12 h post-inoculation and dried at 70 °C for 3 d. Twenty-one-day-old soil-grown cucumber seedlings were inoculated with *B. velezensis* SQR9 or the derived strains at a final concentration of 10^7 cells per ml, and 5 μM YukE or $YukE^{S38C}$ was supplied by thorough irrigation. The roots were collected at 12 h post-inoculation, carefully washed and dried at 70 °C for 3 d. The dried plant tissues were digested with $HNO_3/HClO_4$ (4:1 v/v). The resultant solution was subjected to ICP-MS. For *Arabidopsis*, every treatment included 3 replicates with 24 pooled plants per replicate, and for cucumber plants, each treatment included 4 replicates with 3 pooled plants per replicate.

Growth-promoting effect of YukE and SQR9 on cucumber

Germinated cucumber seedlings were dipped into a cell suspension (10^7 cells per ml) of SQR9 for 1 d and then transferred to pots filled with soil. For treatment with YukE, 5 μM YukE was added to the cell suspension used for inoculation. Each pot had four seedlings as a replicate. The seedlings were cultured in a greenhouse at 28 °C with a 16 h light and 8 h dark photoperiod. The fresh weights of cucumber were recorded after culturing for 20 d. Ten replicates were included for each treatment.

RNA extraction

Root total RNA for RT-qPCR and RNA-seq analyses was extracted using the RNeasy plant mini kit (Qiagen). Bacterial total RNA was extracted using the bacterial RNA kit (OMEGA, Biotek). The extracted RNA was evaluated on a 1% agarose gel, and the concentration and quality (A260/A280) were determined by a NanoDrop ND-2000 spectrophotometer (NanoDrop).

Root RNA-seq

Fifteen-day-old *Arabidopsis* grown in 6-well plates containing 3 ml of 1/2 MS medium was supplied with purified YukE or heat-treated YukE. YukE was added to the rhizosphere at a final concentration of 5 μM. Untreated plants were included as controls. At 1 h, 3 h, 6 h and 24 h post-treatment, roots from the control and all the treated plants were cut and rapidly placed in liquid nitrogen for subsequent RNA extraction. Then, the extracted RNA was used for library preparation and sequencing.

The library was prepared and sequenced on an Illumina HiSeq 4000, and 150 bp paired-end reads were generated at Beijing Allwegene. Clean reads were obtained after quality control and mapped to the reference genome using TopHat2. RNA-seq data were normalized to fragments per kilobase of exon per million fragments mapped (FPKM). Sequence data were deposited in the Sequence Read Archive (SRA) with the accession number PRJNA649312.

Functional enrichment analysis

The *P* value for the comparison of gene expression was calculated using a negative binomial distribution-based test. The false discovery rate (FDR) (*P* adjusted) was calculated using Benjamini–Hochberg correction and the DEGs were screened using an FDR < 0.05. The unique DEGs in the YukE treatment in comparison with the heat-treated YukE treatment were recorded and subjected to DAVID analysis for functional annotation[55,56]. GO enrichment and keyword enrichment were analysed and evaluated using the *P* value and FDR with the Benjamini method. The enriched terms were screened using an FDR < 0.05.

RT-qPCR

The RNA samples were reverse-transcribed to complementary DNA using the PrimeScript RT reagent kit with gDNA Eraser (Takara). SYBR Premix Ex *Taq* (Takara) was used for RT-qPCR with QuantStudio 6 Flex (Applied Biosystems). The following PCR programme was used: cDNA was denatured for 30 s at 95 °C, followed by 40 cycles of 5 s at 95 °C and 34 s at 60 °C. The reference genes used for bacteria and plants were *recA* and *actin*, respectively. The specificity of the amplification was verified using melting curve analysis. Each treatment included 3 replicates.

Reactive oxidative species measurement

For O_2^- measurement in plant roots in response to *B. velezensis* SQR9 and its mutants, roots from 15-day-old *Arabidopsis* plants were inoculated with the bacteria. At 1 h, 3 h, 6 h, 9 h and 22 h post-inoculation, the roots were stained with nitro blue tetrazolium (NBT, 2 mg ml^{-1}) for 2 h and destained with 70% ethanol at 70 °C as described previously[24]. Six replicates were included for each treatment.

PI and FM4-64 staining

For PI and FM4-64 staining, aseptic cultures of 15-day-old *Arabidopsis* Col-0 (after treatment with YukE or bacteria) were washed three times with deionized water. The roots were completely immersed in 10 μg ml^{-1} PI (Sigma–Aldrich) under dark conditions for 10 min or in 2 μM FM4-64

(Thermo Fisher) immediately before confocal laser scanning microscope (CLSM). The whole process was gentle to avoid damage to the roots. The number of nuclei stained by PI was counted manually.

Agrobacterium-mediated transient expression

Transient gene expression assay in *N. benthamiana* mediated by *A. tumefaciens* was performed as previously described[57]. The full-length coding sequence of YukE was cloned into the entry vector pENTR/SD-TOPO and transferred into the binary vector pEarleyGateS101 to form 35S promoter-driven C-terminal fusions with GFP and then transformed into *A. tumefaciens* GV3101. Transformed *Agrobacterium* cells were collected and washed three times with infiltration buffer (10 mM MES, pH 5.5, 10 mM $MgCl_2$) and the cell density was adjusted to an OD_{600} of 0.3. Acetosyringone was added to a final concentration of 200 μM. Then, the mixture was cultured at 30 °C for 3 h with shaking. *Agrobacterium* strains (1 ml) harbouring PM-mCherry (OD_{600} 0.3), p38 (OD_{600} 0.3) and GV3101-YukE-GFP (OD_{600} 0.3) were mixed and infiltrated into 5-week-old *N. benthamiana* leaves. The inoculated plants were kept in the greenhouse for 2 d for subsequent observation[57]. After 48 h, leaf discs of *N. benthamiana* were collected from each infiltrated area to observe the localization of GFP-fusion proteins by CLSM. GFP excitation and emission wavelengths were 488 nm and 530 nm, respectively, and mCherry excitation and emission wavelengths were 561 nm and 610 nm, respectively.

CLSM for *Arabidopsis* inoculated with bacteria

The *yukE* gene was fused with *gfp* at the C terminus to generate SQR9 *yukE::yukE-gfp*. The coding gene of mVENUS was introduced into the genome of SQR9 *yukE::yukE-gfp*. To view the position of *B. velezensis* SQR9 and the secreted YukE in the rhizosphere, 15-day-old *Arabidopsis* seedlings were transferred from a 6-well plate to a laser confocal dish and inoculated with the bacterium at a final concentration of 10^7 cells per ml. A vigorous washing step was included to remove the bacteria and the unattached YukE proteins. The laser confocal dish with the inoculated *Arabidopsis* was placed under the CLSM system (Zeiss LSM880). The green fluorescence and mVENUS fluorescence were monitored following a previously described method[58]. The objective used was a Zeiss EC Plan-Apochromat 20 x/0.8 M27. The excitation and emission wavelengths for GFP, FM4-64, PI and mVENUS were 488 nm and 507 nm, 515 nm and 640 nm, 543 nm and 607 nm, and 514 nm and 537 nm, respectively.

Labelling protein with NBD

NBD labelling of YukE variants was performed following a previously described method[59]. The protein with cysteine residue was mixed with NBD (*N*,*N*′-dimethyl-*N*-(iodoacetyl)-*N*′-(7-nitrobenz-2-OXa-1,3-diazol)-ethylenediamine) at a molar concentration ratio of 1:10 in the dark and incubated at 25 °C for 2 h, followed by passing through a PD-10 desalting column (GE Healthcare packed with Sephadex G-25 medium) to remove the free dye. The NBD-labelled proteins were concentrated by ultrafiltration and stored at −80 °C.

Liposome preparation and detection of NBD fluorescence

For liposome preparation, 1,2-dipalmitoyl-sn-glycero-3-phosphocholine (DPPC) (Avanti Polar Lipids) was fully dissolved in a mixture of chloroform and methanol (volume ratio 6:4) at a concentration of 1 mg ml^{-1} (ref. 60). Subsequently, rotary evaporation in vacuum was performed with the solution at 45°C for 3 h to completely remove the organic solvent and to form a lipid film. Finally, a 30 min ultrasound hydration step was performed in an ice bath with PBS solution, followed by extrusion through a 100 nm nucleopore filter in a mini-extruder (Avanti Polar Lipids).

For real-time fluorescence detection of NBD, 5 μM NBD-labelled proteins were added to 200 μl 0.25 mg ml^{-1} liposomes. In the meantime, labelled proteins were added into PBS solution as a control. Then, NBD fluorescence was immediately detected by an Infinite M200 PRO (Tecan) controlled by Tecan i-control software (v.1.12). The excitation and emission wavelengths for NBD were 488 nm and 544 nm, respectively. Three replicates were included.

Arabidopsis protoplast preparation and CLSM for NBD fluorescence

The protoplast was prepared as previously described[61]. Briefly, leaf and root tissues were cut into 1–3 mm segments from 15-day-old sterile *Arabidopsis* and placed into TVL solution (0.3 M sorbitol and 50 mM $CaCl_2$). Then, the enzyme solution containing 0.5 M sucrose, 10 mM MES, 20 mM $CaCl_2$, 40 mM KCl, 1% cellulase (Onozuka R10) and 1% macerozyme (R-10) were added, followed by vacuum for 30 min in darkness to promote penetration. The solution containing protoplasts was filtered through a 300-mesh nylon mesh after gentle swirling motion at room temperature for 16 h. Next, the W5 solution (2 mM MES pH 5.7, 154 mM NaCl, 125 mM $CaCl_2$ and 5 mM KCl) was gently covered and centrifuged at 100 × *g* for 7 min and the supernatant was carefully removed. The protoplasts were then washed 2–3 times with W5 until the enzymatic solution was completely removed, and the protoplasts were finally dissolved in W5 solution and diluted to 10^4 cells per ml. Then, 5 μM NBD-labelled proteins were added to 100 μl protoplasts, incubated at 25 °C in the dark for 15 h and imaged by a CLSM system. The NBD excitation and emission wavelengths were 488 nm and 544 nm, respectively.

Analysis with ImageJ

The CLSM images for PI and FM4-64 staining and *Agrobacterium*-mediated transient expression were quantitatively analysed using ImageJ (Fiji). Pearson's correlation coefficient for comparisons of fluorophores in every pixel above thresholds (Rcoloc) and Manders' co-localization coefficient above thresholds (tM1, tM2) were calculated using the ImageJ co-localization threshold plugin[62]. The integrated fluorescence density and area of each protoplast were analysed using ImageJ (Fiji) software. The fluorescence intensity of each protoplast was calculated as: fluorescence integrated density of each protoplast/area of each protoplast.

Measurement of iron released from liposomes

Liposomes encapsulating iron ions were generated to verify YukE-induced iron release. Briefly, DPPC was dissolved in chloroform and methanol (volume ratio 6:4) at a concentration of 1 mg ml^{-1}. Lipid films were formed with the mixture by rotary evaporation at 45 °C, followed by a vacuum step to remove residual organic solvents. The dry films were hydrated with 10 mM $FeCl_3$ and 5 mM HEPES, and the hydration mixture was subsequently subjected to seven freeze-thaw cycles with liquid nitrogen and a 55 °C water bath in each cycle, followed by extrusion through a 100 nm Nucleopore filter in a mini-extruder (Avanti Polar Lipids) to generate liposomes encapsulating iron ions. Finally, the buffer of homogenized liposomes was exchanged with 10 mM HEPES and 50 mM NaCl (pH 6.8) by passing through a Sephadex G-25 column (GE Healthcare) to obtain a suspension of liposomes encapsulating $FeCl_3$ in buffer with NaCl.

Calcein blue is a membrane-impermeant fluorescent dye that is used as an iron indicator[60]. The fluorescence of calcein blue could be quenched by iron ions in a dose-dependent manner. For real-time detection of the iron released from the liposomes, YukE and calcein blue (MedChem Express) were added to 200 μl of liposomes to final concentrations of 5 μM and 1.5 μM, respectively. $YukE^{S38C}$-treated and untreated liposomes were included as the negative control and blank control, respectively, while liposomes encapsulating iron ions without calcein blue were included as the fluorescence background. The fluorescence of calcein blue was immediately detected by an microplate reader (Infinite M200 PRO, Tecan) controlled by Tecan i-control software (v.1.12). The excitation and emission wavelengths were 350 nm

and 431 nm, respectively. Five independent replicates were included for each treatment.

Statistical analysis

For intercorrelation analysis of genes in *B. velezensis* SQR9, 72 RNA-seq data sets of *B. velezensis* SQR9 with FPKM values were collected. The FPKM values were then normalized by the sum and transformed to relative log expression values. The Pearson correlation of the transcription between each gene pair was calculated using R (v.3.6). For functional enrichment analysis of the *Arabidopsis* RNA-seq data by DAVID, *P* values were calculated to examine the significance of gene–term enrichment using a modified Fisher's exact test (EASE score); Bonferroni, Benjamini and FDR were exploited to globally correct enrichment *P* values to control family-wide FDR under a certain rate (0.05). For multiple comparisons, one-way analysis of variance (ANOVA) and two-way ANOVA were used. Duncan's multiple-range test ($\alpha = 0.05$) was employed to determine differences among means and was performed using SPSS (v.27.0). Pairwise statistical significance was analysed using Excel (T-Test function). Plotting was performed with GraphPad PRISM (v.9.0).

No data was excluded for the analysis. Data collection and analysis were not performed blind to the conditions of the experiments. No statistical methods were used to pre-determine sample sizes but our sample sizes are similar to those reported in previous publications[63]. Data distribution was assumed to be normal but this was not formally tested. Randomization is not relevant to this study, as all work were exclusively conducted with controlled experiments in which it is only expected that the independent variable will differ between control and experimental groups.

Reporting summary

Further information on research design is available in the Nature Portfolio Reporting Summary linked to this article.

Data availability

Raw data for the plant RNA-seq have been deposited in the Sequence Read Archive (SRA) with the accession number PRJNA649312. Summary data for strains, plasmids and oligonucleotides used in this study can be found in Supplementary Tables 4 and 5. The crystal form of *Geobacillus thermodenitrificans* EsxA could be download with PDB identifier: 3ZBH (https://www.rcsb.org/structure/3ZBH). Other data supporting the findings of the present study are available within the paper, in Extended Data and the Supplementary Information. Source data are provided with this paper.

References

1. Arnaouteli, S., Bamford, N. C., Stanley-Wall, N. R. & Kovács, Á. T. *Bacillus subtilis* biofilm formation and social interactions. *Nat. Rev. Microbiol.* **19**, 600–614 (2021).
2. De Coninck, B., Timmermans, P., Vos, C., Cammue, B. P. A. & Kazan, K. What lies beneath: belowground defense strategies in plants. *Trends Plant Sci.* **20**, 91–101 (2015).
3. Haas, D. & Défago, G. Biological control of soil-borne pathogens by fluorescent pseudomonads. *Nat. Rev. Microbiol.* **3**, 307–319 (2005).
4. Lugtenberg, B. J. J. J., Dekkers, L. & Bloemberg, G. V. Molecular determinants of rhizosphere colonization by *Pseudomonas*. *Annu. Rev. Phytopathol.* **39**, 461–490 (2001).
5. Bulgarelli, D., Schlaeppi, K., Spaepen, S., van Themaat, E. V. L. & Schulze-Lefert, P. Structure and functions of the bacterial microbiota of plants. *Annu. Rev. Plant Biol.* **64**, 807–838 (2013).
6. Siddiqui, Z. A. (Ed) in *PGPR: Biocontrol and Biofertilization* 111–142 (Springer, 2006).
7. Philippot, L., Raaijmakers, J. M., Lemanceau, P. & van der Putten, W. H. Going back to the roots: the microbial ecology of the rhizosphere. *Nat. Rev. Microbiol.* **11**, 789–799 (2013).
8. Pieterse, C. M. J. et al. Induced systemic resistance by beneficial microbes. *Annu. Rev. Phytopathol.* **52**, 347–375 (2014).
9. Harbort, C. J. et al. Root-secreted coumarins and the microbiota interact to improve iron nutrition in *Arabidopsis*. *Cell Host Microbe* **28**, 825–837 (2020).
10. Verbon, E. H. et al. Iron and immunity. *Annu. Rev. Phytopathol.* **55**, 355–375 (2017).
11. Herlihy, J. H., Long, T. A. & McDowell, J. M. Iron homeostasis and plant immune responses: recent insights and translational implications. *J. Biol. Chem.* **295**, 13444–13457 (2020).
12. Xu, Z. et al. Antibiotic bacillomycin D affects iron acquisition and biofilm formation in *Bacillus velezensis* through a Btr-mediated FeuABC-dependent pathway. *Cell Rep.* **29**, 1192–1202.e5 (2019).
13. Chang, J. H., Desveaux, D. & Creason, A. L. The ABCs and 123s of bacterial secretion systems in plant pathogenesis. *Annu. Rev. Phytopathol.* **52**, 317–345 (2014).
14. Costa, T. R. D. et al. Secretion systems in Gram-negative bacteria: structural and mechanistic insights. *Nat. Rev. Microbiol.* **13**, 343–359 (2015).
15. Abdallah, A. M. et al. Type VII secretion — Mycobacteria show the way. *Nat. Rev. Microbiol.* **5**, 883–891 (2007).
16. Conrad, W. H. et al. Mycobacterial ESX-1 secretion system mediates host cell lysis through bacterium contact-dependent gross membrane disruptions. *Proc. Natl Acad. Sci. USA* **114**, 1371–1376 (2017).
17. De Leon, J. et al. *Mycobacterium tuberculosis* ESAT-6 exhibits a unique membrane-interacting activity that is not found in its ortholog from non-pathogenic *Mycobacterium smegmatis*. *J. Biol. Chem.* **287**, 44184–44191 (2012).
18. Zhang, Q., Aguilera, J., Reyes, S. V. & Sun, J. Membrane insertion of *Mycobacterium tuberculosis* EsxA in cultured lung epithelial cells. Preprint at *bioRxiv* https://doi.org/10.1101/2020.04.09.035238 (2020).
19. Baptista, C., Barreto, H. C. & São-José, C. High levels of DegU-P activate an Esat-6-like secretion system in *Bacillus subtilis*. *PLoS ONE* **8**, e67840 (2013).
20. Huppert, L. A. et al. The ESX system in *Bacillus subtilis* mediates protein secretion. *PLoS ONE* **9**, e96267 (2014).
21. Sysoeva, T. A., Zepeda-Rivera, M. A., Huppert, L. A. & Burton, B. M. Dimer recognition and secretion by the ESX secretion system in *Bacillus subtilis*. *Proc. Natl Acad. Sci. USA* **111**, 7653–7658 (2014).
22. Li, Y. et al. Volatile compounds from beneficial rhizobacteria *Bacillus* spp. promote periodic lateral root development in *Arabidopsis*. *Plant Cell Environ.* **44**, 1663–1678 (2021).
23. Liu, Y. et al. Identification of root-secreted compounds involved in the communication between cucumber, the beneficial *Bacillus amyloliquefaciens*, and the soil-borne pathogen *Fusarium oxysporum*. *Mol. Plant Microbe Interact.* **30**, 53–62 (2017).
24. Zhang, H. et al. *Bacillus velezensis* tolerance to the induced oxidative stress in root colonization contributed by the two-component regulatory system sensor ResE. *Plant Cell Environ.* **44**, 3094–3102 (2021).
25. Xiong, Q. et al. Quorum sensing signal autoinducer-2 promotes root colonization of *Bacillus velezensis* SQR9 by affecting biofilm formation and motility. *Appl. Microbiol. Biotechnol.* **104**, 7177–7185 (2020).
26. Liu, Y. et al. Induced root-secreted D-galactose functions as a chemoattractant and enhances the biofilm formation of *Bacillus velezensis* SQR9 in an McpA-dependent manner. *Appl. Microbiol. Biotechnol.* **104**, 785–797 (2020).
27. Dong, X. et al. Synthesis and detoxification of nitric oxide in the plant beneficial rhizobacterium *Bacillus amyloliquefaciens* SQR9 and its effect on biofilm formation. *Biochem. Biophys. Res. Commun.* **503**, 784–790 (2018).

28. Liu, Y. et al. Root-secreted spermine binds to *Bacillus amyloliquefaciens* SQR9 histidine kinase KinD and modulates biofilm formation. *Mol. Plant Microbe Interact.* **33**, 423–432 (2020).
29. Colangelo, E. P. & Guerinot, M. L. The essential basic helix-loop-helix protein FIT1 is required for the iron deficiency response. *Plant Cell* **16**, 3400–3412 (2004).
30. Trapet, P. L. et al. Mechanisms underlying iron deficiency-induced resistance against pathogens with different lifestyles. *J. Exp. Bot.* **72**, 2231–2241 (2021).
31. Hsiao, P. Y., Cheng, C. P., Koh, K. W. & Chan, M. T. The *Arabidopsis* defensin gene, AtPDF1.1, mediates defence against *Pectobacterium carotovorum* subsp. *carotovorum* via an iron-withholding defence system. *Sci. Rep.* **7**, 9175 (2017).
32. Xing, Y. et al. Bacterial effector targeting of a plant iron sensor facilitates iron acquisition and pathogen colonization. *Plant Cell* **33**, 2015–2031 (2021).
33. Dangol, S., Chen, Y., Hwang, B. K. & Jwa, N. S. Iron- and reactive oxygen species-dependent ferroptotic cell death in rice–*Magnaporthe oryzae* interactions. *Plant Cell* **31**, 189–209 (2019).
34. Sun, L. et al. Restriction of iron loading into developing seeds by a YABBY transcription factor safeguards successful reproduction in *Arabidopsis*. *Mol. Plant* **14**, 1624–1639 (2021).
35. Pescador, L. et al. Nitric oxide signalling in roots is required for MYB72-dependent systemic resistance induced by *Trichoderma* volatile compounds in *Arabidopsis*. *J. Exp. Bot.* **73**, 584–595 (2022).
36. Yu, K. et al. Rhizosphere-associated *Pseudomonas* suppress local root immune responses by gluconic acid-mediated lowering of environmental pH. *Curr. Biol.* **29**, 3913–3920.e4 (2019).
37. Zamioudis, C., Hanson, J. & Pieterse, C. M. J. ß-glucosidase BGLU42 is a MYB72-dependent key regulator of rhizobacteria-induced systemic resistance and modulates iron deficiency responses in *Arabidopsis* roots. *New Phytol.* **204**, 368–379 (2014).
38. Zamioudis, C. et al. Rhizobacterial volatiles and photosynthesis-related signals coordinate MYB72 expression in *Arabidopsis* roots during onset of induced systemic resistance and iron-deficiency responses. *Plant J.* **84**, 309–322 (2015).
39. Ma, Y., Keil, V. & Sun, J. Characterization of *Mycobacterium tuberculosis* EsxA membrane insertion: roles of N- and C-terminal flexible arms and central helix-turn-helix motif. *J. Biol. Chem.* **290**, 7314–7322 (2015).
40. Gröschel, M. I., Sayes, F., Simeone, R., Majlessi, L. & Brosch, R. ESX secretion systems: mycobacterial evolution to counter host immunity. *Nat. Rev. Microbiol.* **14**, 677–691 (2016).
41. Refai, A. et al. Two distinct conformational states of *Mycobacterium tuberculosis* virulent factor early secreted antigenic target 6 kDa are behind the discrepancy around its biological functions. *FEBS J.* **282**, 4114–4129 (2015).
42. Casabona, M. G. et al. Functional analysis of the EsaB component of the *Staphylococcus aureus* type VII secretion system. *Microbiology* **163**, 1851–1863 (2017).
43. Isaac, D. T., Laguna, R. K., Valtz, N. & Isberg, R. R. MavN is a *Legionella pneumophila* vacuole-associated protein required for efficient iron acquisition during intracellular growth. *Proc. Natl Acad. Sci. USA* **112**, E5208–E5217 (2015).
44. Ravet, K. et al. Ferritins control interaction between iron homeostasis and oxidative stress in *Arabidopsis*. *Plant J.* **57**, 400–412 (2009).
45. Khan, A., Singh, P. & Srivastava, A. Synthesis, nature and utility of universal iron chelator – siderophore: a review. *Microbiol. Res.* **212–213**, 103–111 (2018).
46. Kremer, J. M. et al. Peat-based gnotobiotic plant growth systems for *Arabidopsis* microbiome research. *Nat. Protoc.* **16**, 2450–2470 (2021).
47. Feng, H. et al. Identification of chemotaxis compounds in root exudates and their sensing chemoreceptors in plant-growth-promoting rhizobacteria *Bacillus amyloliquefaciens* SQR9. *Mol. Plant Microbe Interact.* **31**, 995–1005 (2018).
48. Bulgarelli, D. et al. Revealing structure and assembly cues for *Arabidopsis* root-inhabiting bacterial microbiota. *Nature* **488**, 91–95 (2012).
49. Qiu, M. et al. De-coupling of root–microbiome associations followed by antagonist inoculation improves rhizosphere soil suppressiveness. *Biol. Fertil. Soils* **50**, 217–224 (2014).
50. Inoue, T. et al. Genome-wide screening of genes required for swarming motility in *Escherichia coli* K-12. *J. Bacteriol.* **189**, 950–957 (2007).
51. De Meutter, J. & Goormaghtigh, E. Protein structural denaturation evaluated by MCR-ALS of protein microarray FTIR spectra. *Anal. Chem.* **93**, 13441–13449 (2021).
52. Liu, F., Shah, D. S. & Gadd, G. M. Role of protein in fungal biomineralization of copper carbonate nanoparticles. *Curr. Biol.* **31**, 358–368.e3 (2021).
53. Cai, S. & Singh, B. R. A distinct utility of the amide III infrared band for secondary structure estimation of aqueous protein solutions using partial least squares methods. *Biochemistry* **43**, 2541–2549 (2004).
54. Lei, G. J. et al. Abscisic acid alleviates iron deficiency by promoting root iron reutilization and transport from root to shoot in *Arabidopsis*. *Plant Cell Environ.* **37**, 852–863 (2014).
55. Huang, D. W., Sherman, B. T. & Lempicki, R. A. Systematic and integrative analysis of large gene lists using DAVID bioinformatics resources. *Nat. Protoc.* **4**, 44–57 (2009).
56. Sherman, B. T. et al. DAVID: a web server for functional enrichment analysis and functional annotation of gene lists (2021 update). *Nucleic Acids Res.* **50**, W216–W221 (2022).
57. Wei, H. L., Chakravarthy, S., Worley, J. N. & Collmer, A. Consequences of flagellin export through the type III secretion system of *Pseudomonas syringae* reveal a major difference in the innate immune systems of mammals and the model plant *Nicotiana benthamiana*. *Cell. Microbiol.* **15**, 601–618 (2013).
58. Emonet, A. et al. Spatially restricted immune responses are required for maintaining root meristematic activity upon detection of bacteria. *Curr. Biol.* **31**, 1012–1028.e7 (2021).
59. Oroz, J. et al. Structure and pro-toxic mechanism of the human Hsp90/PPIase/Tau complex. *Nat. Commun.* **9**, 4532 (2018).
60. Yavlovich, A., Singh, A., Blumenthal, R. & Puri, A. A novel class of photo-triggerable liposomes containing DPPC:DC 8,9PC as vehicles for delivery of doxorubcin to cells. *Biochim. Biophys. Acta* **1808**, 117–126 (2011).
61. Chen, D. et al. S-acylation of P2K1 mediates extracellular ATP-induced immune signaling in *Arabidopsis*. *Nat. Commun.* **12**, 2750 (2021).
62. Atakpa, P., Thillaiappan, N. B., Mataragka, S., Prole, D. L. & Taylor, C. W. IP3 receptors preferentially associate with ER-lysosome contact sites and selectively deliver Ca^{2+} to lysosomes. *Cell Rep.* **25**, 3180–3193.e7 (2018).
63. Cao, Z., Casabona, M. G., Kneuper, H., Chalmers, J. D. & Palmer, T. The type VII secretion system of *Staphylococcus aureus* secretes a nuclease toxin that targets competitor bacteria. *Nat. Microbiol.* **2**, 16183 (2016).

Acknowledgements

This work was funded by the National Natural Science Foundation of China (32070104, Y.L.), the National Natural Science Foundation of China (32172661, R.Z.), the National Key Research and Development Programme (2022YFF1001804, R.Z.), the National Key Research and Development Program (2021YFF1000400, Y.L. and R.Z.), the Central Public-interest Scientific Institution Basal Research Fund

(No. Y2022QC15, Y.L.), and the Agricultural Science and Technology Innovation Program (CAAS-ZDRW202308, Y.L.). We thank H. Wei and J. Li of the Institute of Agricultural Resources and Regional Planning, Chinese Academy of Agricultural Sciences, for providing the strains and plasmid used in the *Agrobacterium*-mediated transient expression experiment; and X. Shen of the College of Life Sciences, Northwest A&F University, for help with editing the manuscript.

Author contributions

Y.L. and R.Z. conceptualized the project; X. Shu, L.C. and G.L conducted formal analysis; Y.L., X. Shu, L.C., H.Z. and X. Sun conducted the investigation; H.F. and Q.X. performed verification; Y.L. and L.C. wrote the original draft; L.C., C.M.J.P. and R.Z. reviewed and edited the paper; X. Shu, W.X. and Z.X. performed visualization; Y.L., C.M.J.P. and R.Z. supervised the work; N.Z. and Q.S. administered the project; Y.L. and R.Z acquired funding. All authors read and approved the submitted version.

Competing interests

The authors declare no competing interests.

Additional information

Extended data is available for this paper at https://doi.org/10.1038/s41564-023-01402-1.

Supplementary information The online version contains supplementary material available at https://doi.org/10.1038/s41564-023-01402-1.

Correspondence and requests for materials should be addressed to Yunpeng Liu or Ruifu Zhang.

Peer review information *Nature Microbiology* thanks Edith Houben and the other, anonymous, reviewer(s) for their contribution to the peer review of this work.

https://doi.org/10.1038/s41564-023-01402-1

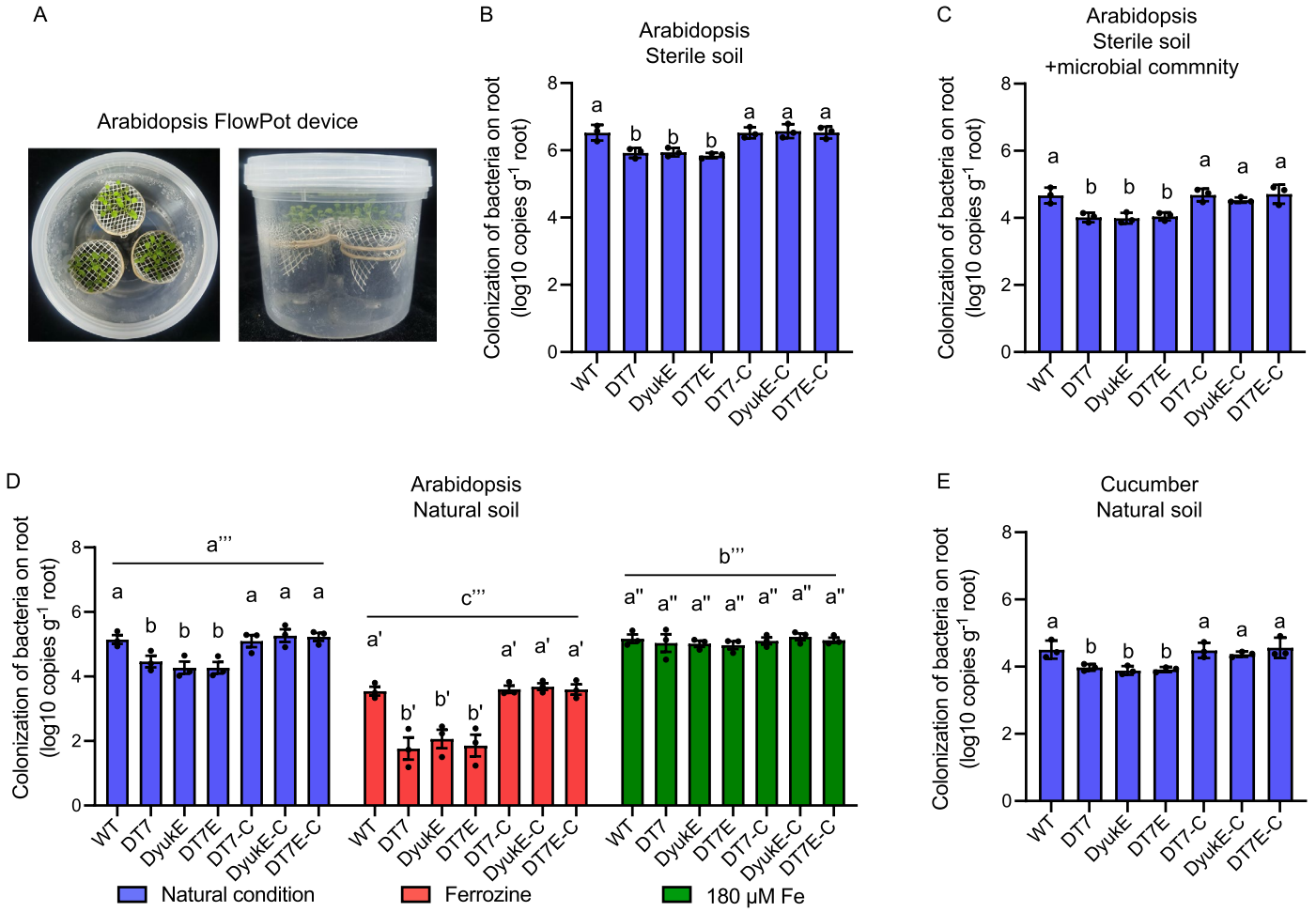

Extended Data Fig. 1 | Colonization of roots of *Arabidopsis* and cucumber grown in soil. WT and the derived strains were introduced with gfp fragments in their genomes for specific detection by qPCR in soil. Bacteria were inoculated to a final concentration of 10^7 cells/mL. DNA of the rhizosphere soil was extracted at 2 days post-inoculation. qRT–PCR was used to measure the copies of the gfp fragment. (A) The gnotobiotic FlowPot device was used to grow Arabidopsis in soil. (B-D) Root colonization of Arabidopsis grown in sterile soil (B), in sterile soil with a microbial community extracted from natural soil (C) and in natural soil (D). Ferrozine and excess iron were supplied at the mean time of inoculation at final concentrations of 300 μM and 180 μM, respectively, when necessary. (E) Root colonization of cucumber grown in natural soil. Fifteen-day-old *Arabidopsis* Col-0 plants and 21-day-old cucumber plants were used for the colonization assay. Error bars indicate the standard errors. Three replicates were included for each strain. Different letters above the column indicate significant differences (two-side one-way ANOVA or two-way ANOVA with Duncan's multiple-range tests, $\alpha = 0.05$, for (B C and E): $P < 0.001$, $P < 0.001$, $P < 0.001$, for the two-way ANOVA in (D), $P < 0.001$, for the one-way ANOVA in (D), from left to right, $P < 0.001$, $P < 0.001$, $P < 0.001$).

https://doi.org/10.1038/s41564-023-01402-1

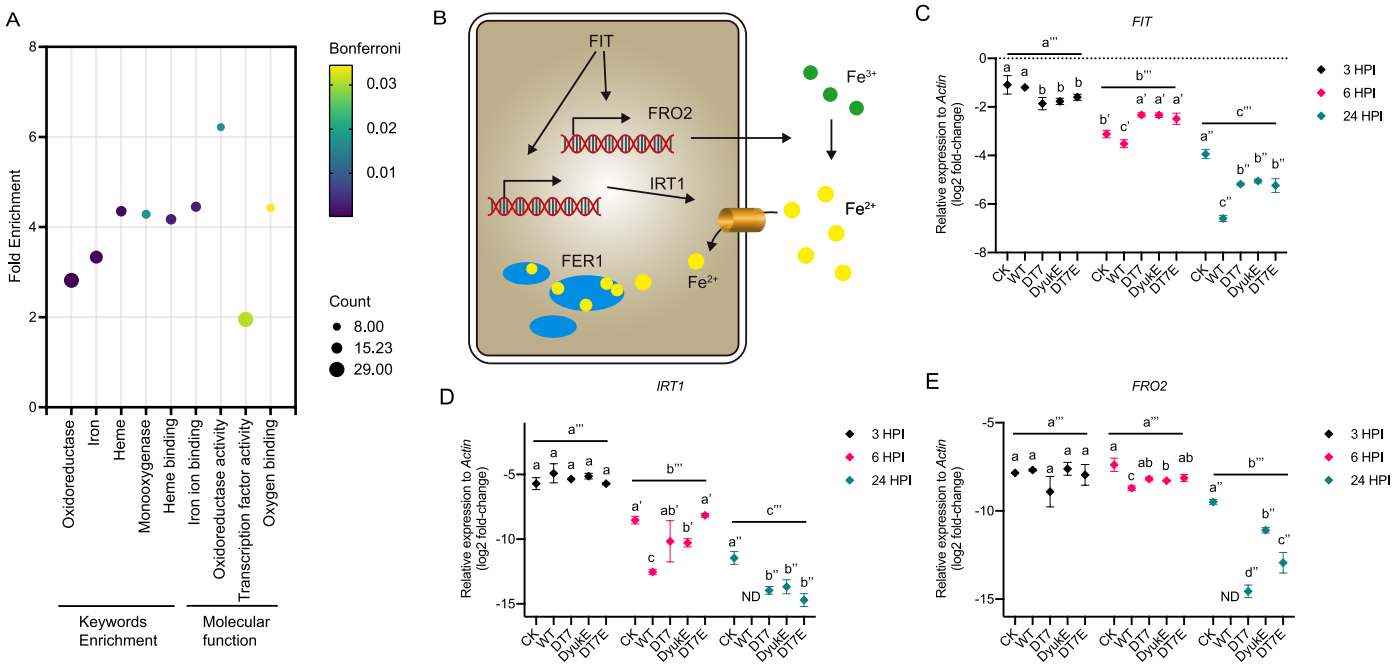

Extended Data Fig. 2 | Effect of the *B. velezensis* SQR9 type VII secretion system (T7SS) on the transcription of iron acquisition genes in 15-day-old *Arabidopsis*. (A) Functional enrichment of the DEGs in the YukE treatment but not in the heat-treated YukE treatment. Briefly, 5 μM purified YukE or heat-treated YukE was added to the plant medium, and RNA-seq was performed at 1 h, 3 h, 6 h and 24 h post-treatment. The FPKM value of each gene in the YukE or heat-treated YukE treatment was compared with that of untreated plants to identify the DEGs. Then, DEGs in the YukE and heat-treated YukE treatments were compared to identify the DEGs present in the YukE treatment but not in the heat-treated YukE treatment. These DEGs were then subjected to functional enrichment analysis using DAVID (https://david.ncifcrf.gov). (B) The iron acquisition pathway in *Arabidopsis*. (C-E) Relative expression of *FIT* (C), *IRT1* (D), and *FRO2* (E) in 15-day-old *Arabidopsis* roots in response to wild-type *B. velezensis* SQR9 and the mutants DT7, DyukE and DT7E measured by qRT–PCR. CK indicates the untreated plant. Roots were harvested at 3, 6 and 24 h post-inoculation, respectively. *Actin* served as a reference. Data are presented as mean values +/- SEM (n = 3). Different letters above the column indicate significant differences (two-side one-way ANOVA or two-way ANOVA with Duncan's multiple-range tests, $\alpha = 0.05$, for one-way ANOVA in (C-E), $P = 0.258$, $P = 0.001$, $P < 0.001$, $P = 0.560$, $P = 0.003$, $P = 0.008$, $P = 0.307$, $P = 0.009$, $P < 0.001$, for all the two-way ANOVA in (C-E), $P < 0.001$). This experiment was repeated three times with similar results.

https://doi.org/10.1038/s41564-023-01402-1

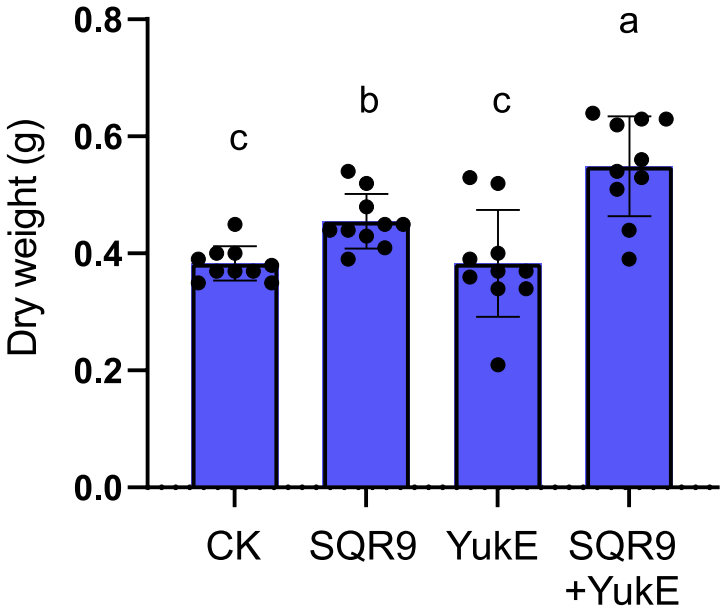

Extended Data Fig. 3 | YukE enhances the growth-promoting effect of *B. velezensis* SQR9 on cucumber. CK indicates the untreated plant. Cucumber was inoculated by dipping the root into a cell suspension (10^7 cells/mL) with or without 5 μM YukE for 1 day before transplanting into soil. Data are presented as mean values +/- SEM (n = 10). Different letters above the column indicate significant differences (two-side one-way ANOVA with Duncan's multiple-range tests, $\alpha = 0.05$, $P < 0.001$). This experiment was repeated twice with similar results.

https://doi.org/10.1038/s41564-023-01402-1

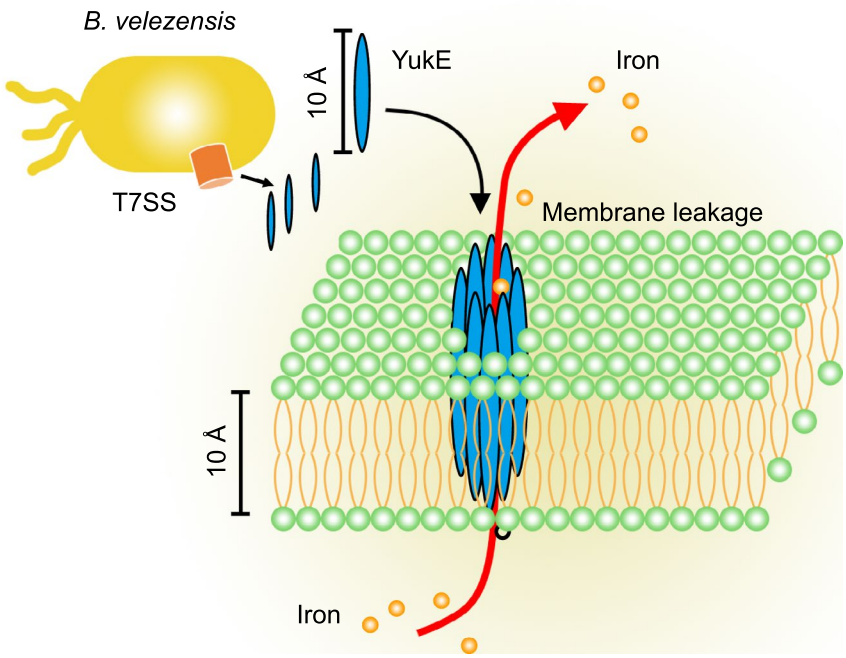

Extended Data Fig. 4 | Model for the role of YukE in the decrease in root iron content. The predicted structure of YukE consists of two helices with a helix-turn-helix motif (WXG motif). The protein was structured as a dimer in vivo and in vitro. The length of the protein is 10.1 Å. The thickness of the phospholipid bilayer is approximately 10 Å. YukE may be inserted into the phospholipid bilayer to cause iron leakage from root cells.

https://doi.org/10.1038/s41564-023-01402-1

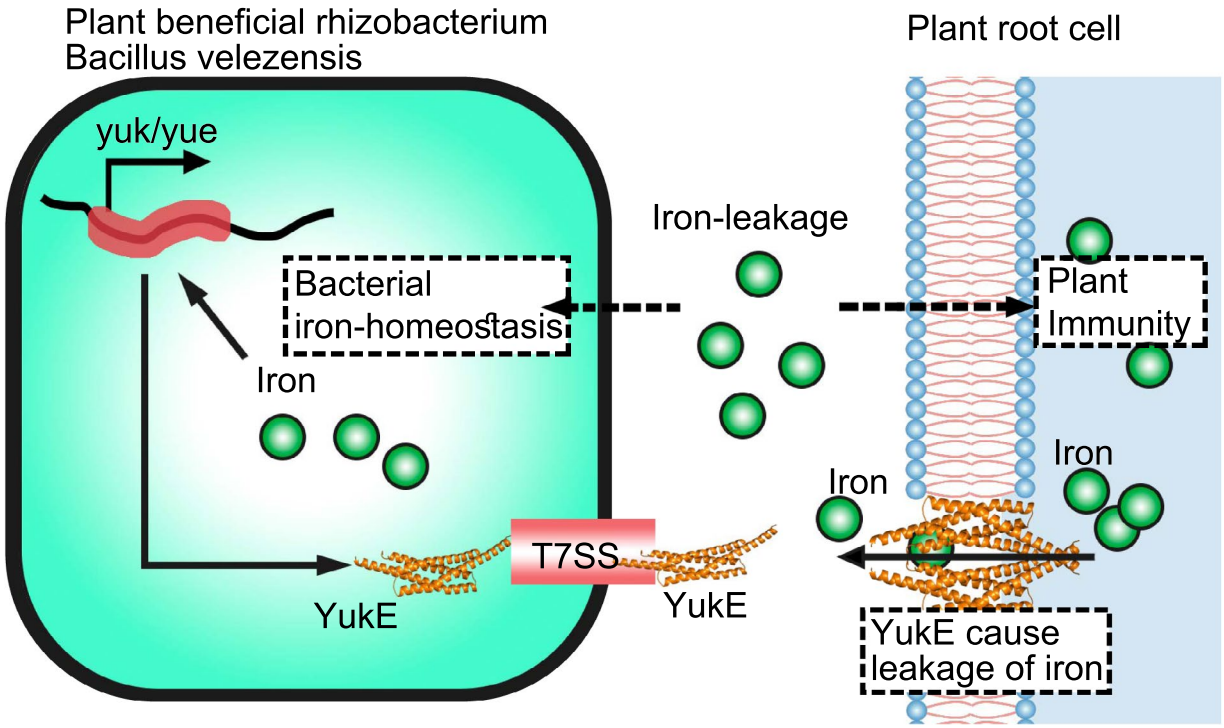

Extended Data Fig. 5 | Model of T7SS function in the interaction of *B. velezensis* SQR9 and plant cells.

https://doi.org/10.1038/s41564-023-01402-1

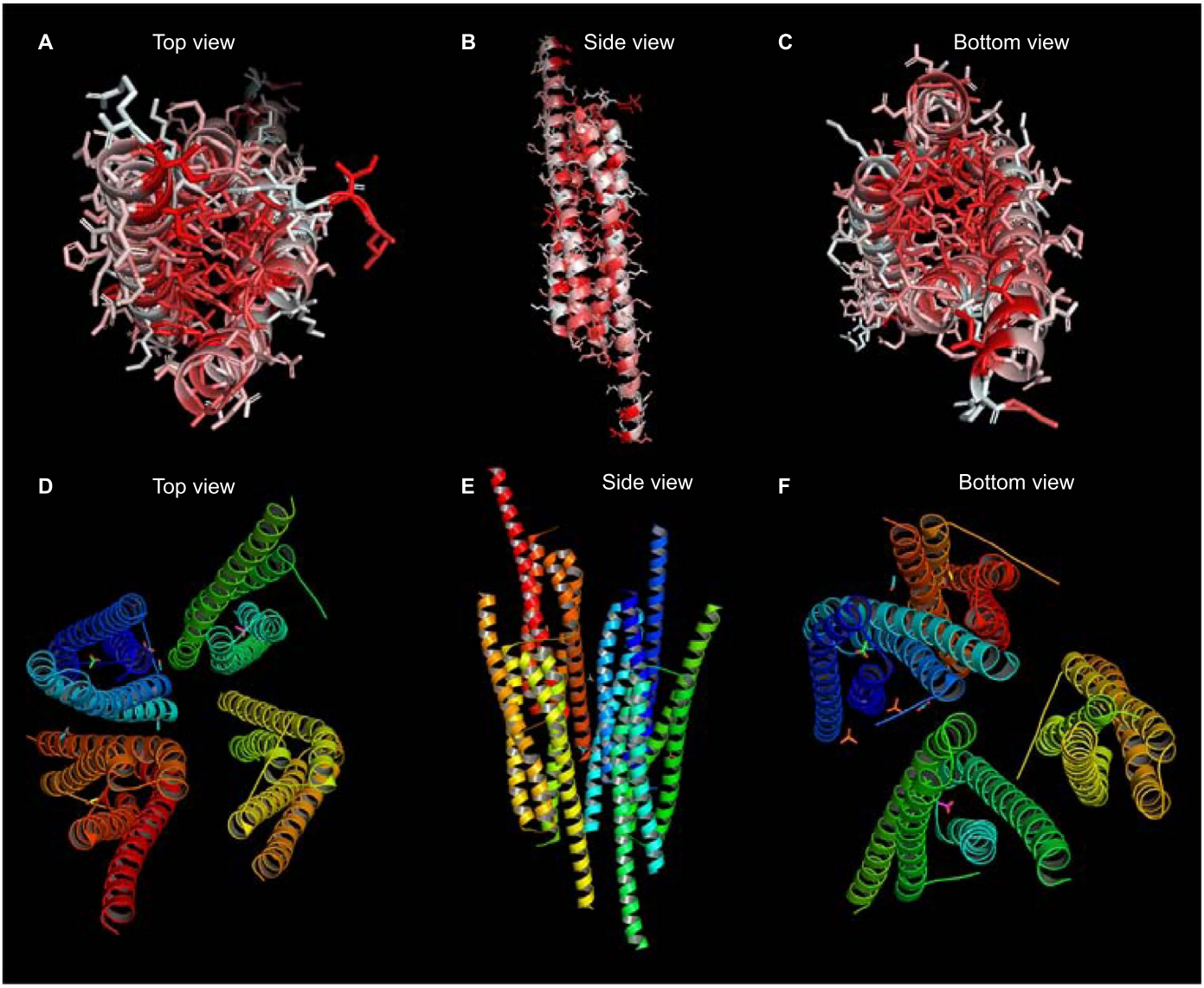

Extended Data Fig. 6 | Protein structures of YukE and EsxA. (A-C) Structure of the YukE homodimer built by Swiss-model using EsxA of *M. tuberculosis* as the template. The polarity of the residues is colored. Red indicates a higher polarity calculated by PyMOL (V. 2.4.1). (D-F) Asymmetric unit of EsxA from *Geobacillus thermodenitrificans*. Different colors indicate different molecules.

nature portfolio

Corresponding author(s): Yunpeng Liu, Ruifu Zhang

Last updated by author(s): Apr 25, 2023

Reporting Summary

Nature Portfolio wishes to improve the reproducibility of the work that we publish. This form provides structure for consistency and transparency in reporting. For further information on Nature Portfolio policies, see our Editorial Policies and the Editorial Policy Checklist.

Statistics

For all statistical analyses, confirm that the following items are present in the figure legend, table legend, main text, or Methods section.

n/a	Confirmed	
☐	☒	The exact sample size (*n*) for each experimental group/condition, given as a discrete number and unit of measurement
☐	☒	A statement on whether measurements were taken from distinct samples or whether the same sample was measured repeatedly
☐	☒	The statistical test(s) used AND whether they are one- or two-sided *Only common tests should be described solely by name; describe more complex techniques in the Methods section.*
☒	☐	A description of all covariates tested
☐	☒	A description of any assumptions or corrections, such as tests of normality and adjustment for multiple comparisons
☐	☒	A full description of the statistical parameters including central tendency (e.g. means) or other basic estimates (e.g. regression coefficient) AND variation (e.g. standard deviation) or associated estimates of uncertainty (e.g. confidence intervals)
☐	☒	For null hypothesis testing, the test statistic (e.g. *F*, *t*, *r*) with confidence intervals, effect sizes, degrees of freedom and *P* value noted *Give P values as exact values whenever suitable.*
☒	☐	For Bayesian analysis, information on the choice of priors and Markov chain Monte Carlo settings
☒	☐	For hierarchical and complex designs, identification of the appropriate level for tests and full reporting of outcomes
☐	☒	Estimates of effect sizes (e.g. Cohen's *d*, Pearson's *r*), indicating how they were calculated

Our web collection on statistics for biologists contains articles on many of the points above.

Software and code

Policy information about availability of computer code

Data collection	Zeiss LSM880 system, Tecan i-control
Data analysis	The Pearson correlation of the transcription between each gene pair was calculated by R (v3.6).The integrated fluorescence density, area of each protoplast and fluorecence colocalization were analyzed using ImageJ (Fiji, v1.53) software. GraphPad PRISM v9 (GraphPad Software) was used for plotting. Statistical test was performed using SPSS Statistics 27 and Excel (v2303) .

For manuscripts utilizing custom algorithms or software that are central to the research but not yet described in published literature, software must be made available to editors and reviewers. We strongly encourage code deposition in a community repository (e.g. GitHub). See the Nature Portfolio guidelines for submitting code & software for further information.

Data

Policy information about availability of data

All manuscripts must include a data availability statement. This statement should provide the following information, where applicable:

- Accession codes, unique identifiers, or web links for publicly available datasets
- A description of any restrictions on data availability
- For clinical datasets or third party data, please ensure that the statement adheres to our policy

Raw data for the plant RNA-seq have been deposited in the Sequence Read Archive (SRA) with the accession number PRJNA649312. Summary data for strains, plasmids and oligonucleotides used in this study can be found in Supplementary Table 4 and 5. Crystal form of Geobacillus thermodenitrificans EsxA could be

download with PDB identifier: 3ZBH. Other data supporting the findings of the present study are available within this article, in Extended Data and the Supplementary Information. Source data are provided with this paper.

Human research participants

Policy information about studies involving human research participants and Sex and Gender in Research.

Reporting on sex and gender	Not applicable
Population characteristics	Not applicable
Recruitment	Not applicable
Ethics oversight	Not applicable

Note that full information on the approval of the study protocol must also be provided in the manuscript.

Field-specific reporting

Please select the one below that is the best fit for your research. If you are not sure, read the appropriate sections before making your selection.

☒ Life sciences ☐ Behavioural & social sciences ☐ Ecological, evolutionary & environmental sciences

For a reference copy of the document with all sections, see nature.com/documents/nr-reporting-summary-flat.pdf

Life sciences study design

All studies must disclose on these points even when the disclosure is negative.

Sample size	We did not perform a calculation for sample size, but we made sure that a sufficient number of replicates were taken following previous experience with these types of experimental data (DOI: 10.1038/nmicrobiol.2016.183). To ensure the reproducibility, some experiments were performed for several times with relevant independent replicates for each time of experiment, the detailed times of experiment were stated in the paper.
Data exclusions	No data was excluded.
Replication	All the root colonization experiments in hydroponic condition were performed with 6 replicates. All the biofilm formation experiments were performed with 4 replicates. All the bacterial iron content measurements were performed with 3 replicates. All the bacterial growth measurements were performed with 6 replicates. All plant iron content measurements were performed with 3 replicates, for each replicates, at least 12 plants were pooled. Plant RNA-seq was performed with 3 replicates. The qPCR was performed with 3 replicates. The ROS measurement was performed with 6 replicates. The liposome-based iron leakage experiment was performed with 5 replicates. The experiments with NBD-labeled YukE was performed with 3 replicates. All attempts at replication was successful for all the experiment.
Randomization	This is not relevant to our study, as all work were exclusively conducted with controlled experiments in which it is only expected that the independent variable will differ between control and experimental groups.
Blinding	No animal study, clinical data or study that require blinding was conducted.

Reporting for specific materials, systems and methods

We require information from authors about some types of materials, experimental systems and methods used in many studies. Here, indicate whether each material, system or method listed is relevant to your study. If you are not sure if a list item applies to your research, read the appropriate section before selecting a response.

Materials & experimental systems

n/a	Involved in the study
☐	☒ Antibodies
☒	☐ Eukaryotic cell lines
☒	☐ Palaeontology and archaeology
☒	☐ Animals and other organisms
☒	☐ Clinical data
☒	☐ Dual use research of concern

Methods

n/a	Involved in the study
☒	☐ ChIP-seq
☒	☐ Flow cytometry
☒	☐ MRI-based neuroimaging

Antibodies

Antibodies used	The polyclonal anti-YukE and anti-RpoD (as internal control) antibodies were generated by AtaGenix Technology Company (Wuhan, China) and used with the dilution of 1:1000. HRP, Goat Anti-Rabbit IgG was used with the dilution of 1:10000 (Abbkine, Catalog No: A21020)
Validation	The purified Polyclonal antibody for YukE and RpoD was verified by western blot with purified YukE and RpoD, and with the cell lysis, the supernatant of the bacteria culture. Single band was observed for these experiment. The titer was verified by ELISA.